NASA/DLR Design Challenge 2018

Team RWTH Aachen University

AixBox One

RWTH Aachen University
Institute of Aerospace Systems
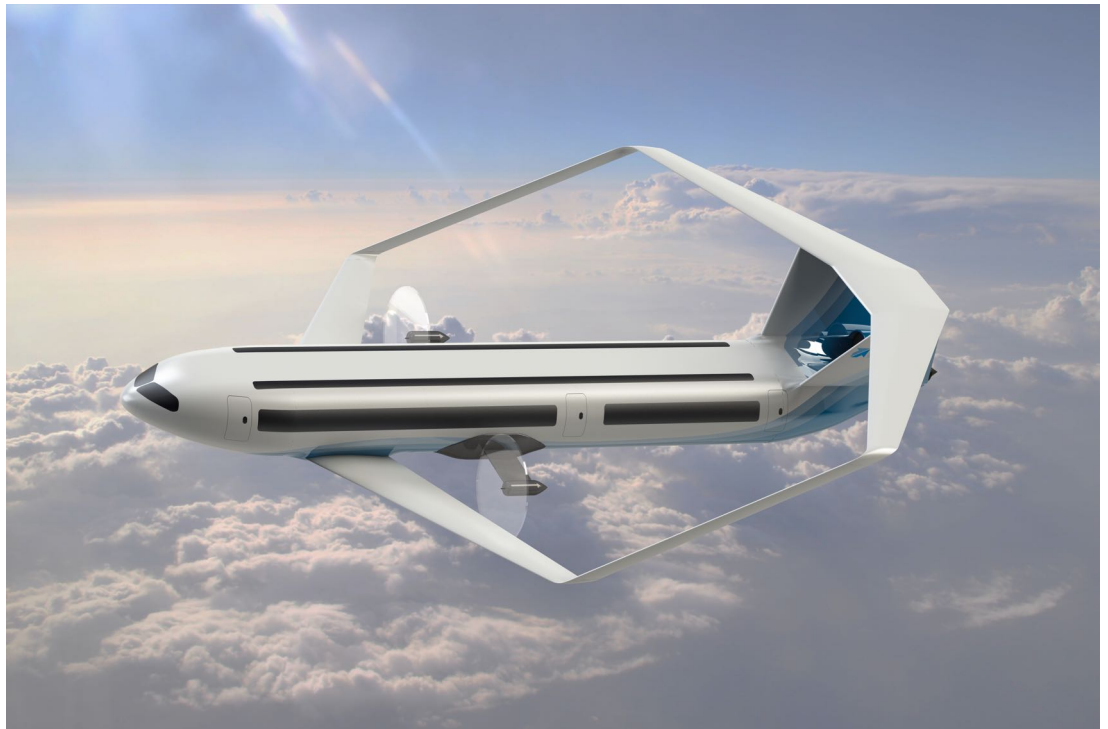
Members:

Hendrik Fuest (Team Leader)	hendrik.fuest@rwth-aachen.de
Joel Rösick	joel.roesick@rwth-aachen.de
Lara Eisler	lara.eisler@rwth-aachen.de
Marc-Antoine Le Gars	marc.antoine.le.gars@rwth-aachen.de
Philipp Podzus	philipp.podzus@rwth-aachen.de
Thomas Lürkens	thomas.luerkens@rwth-aachen.de

Academic Advisors:

Miguel Yael Pereda Albarrán, M.Sc.
Univ.-Prof. Dr.-Ing. Eike Stumpf

This project is submitted on July 1st, 2018

Institut für Luft- & Raumfahrtsysteme | Wüllnerstraße 7, 52062 Aachen   **415310**
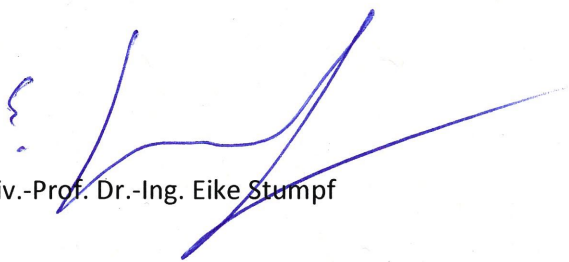
**Univ.-Prof. Dr.-Ing.
Eike Stumpf**

Wüllnerstraße 7
52062 Aachen
GERMANY
Telefon: +49 241 80-96801
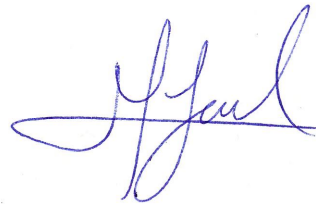Fax: +49 241 80-92233

stumpf@ilr.rwth-aachen.de

22.06.2018

Attestation for Submission

The hereby submitted project work has been confirmed by the Head of Institute of Aerospace Systems (ILR) and is endorsed for the submission in the Design Challenge 2018. The work has been done independently from currently enrolled students from RWTH Aachen University without further assistance of our institute.

Univ.-Prof. Dr.-Ing. Eike Stumpf   Mr. Pereda Albarrán M.Sc.

Team Members

Surname	Name	Field of study
Eisler	Lara	Bachelor's student in Environmental Engineering, 8th Semester
Fuest	Hendrik	Master's student in Aerospace Engineering, 3rd Semester
Le Gars	Marc-Antoine	Master's student in Aerospace Engineering, 1st Semester
Lürkens	Thomas	Master's student in Aerospace Engineering, 3rd Semester
Podzus	Philipp	Master's student in Aerospace Engineering, 3rd Semester
Rösick	Joel	Bachelor's student in Mechanical Engineering, 6th Semester

Abstract

Air traffic has been growing steadily for decades. Recent studies confirm the continuation of this trend. Increasing awareness for environmental pollution associated with air-transport make the development of new aircraft necessary, which can meet the challenges that the aviation industry will have to face in the future. These circumstances call for innovative solutions. The joint NASA/DLR Design Challenge encourages students to propose aircraft designs to deal with these challenges. The primary constraints of the NASA/DLR Design Challenge 2018 are an entry into service in the year 2045 with a minimum decrease in energy consumption of 60 %. The AixBox One is a conceptual short and medium-haul aircraft designed by students from RWTH Aachen University, which meets and exceeds these requirements. A double-bubble fuselage lifted by a boxwing is selected to cope with growing passenger numbers. In this sense, the number of passengers was increased to 264 in a 2-class configuration. Since cruise represents the longest flight phase, the engines are dimensioned for the required cruise thrust. To provide the required thrust during takeoff and climb, a revolutionary system, the AixBox Booster is developed. This is an autonomous aircraft that attaches to AixBox One's fuselage to provide the extra thrust needed during takeoff and climb. Then it returns to the airport automatically. Concerning the reduction of NOx emissions around the airport, AixBox Booster is equipped with an electric powertrain. Further, to reduce weight and noise emission, a ground based landing system is implemented to replace the landing gear. The combination of a novel configuration, the AixBox Booster system and other technical improvements allow for a 67 % reduction in consumed energy for an average mission profile.

Acknowledgments

Contents

List of Figures

List of Tables

Nomenclature

<div align="center">**Abbreviations**</div>

BGSV	Booster ground support vehicle
BLI	Boundary layer ingestion
BM	Bending moment
BPR	Bypass ratio
BWB	Blended wing body
CC	Combustion chamber
CG	Center of gravity
DB	Double-Bubble fuselage
ICAO	International Civil Aviation Organization
MEW	Manufacturer's Empty Weight
MTOW	Maximum Take-Off Weight
MZFM	Maximum Zero Fuel Mass
OEW	Operating Empty Weight
PAX	Passengers
TLARs	Top Level Aircraft Requirements
TSFC	Thrust specific fuel consumption

<div align="center">**Symbols**</div>

α	$[\ ^\circ\ ]$	Angle of attack
$\bar{c}$	$[\ \text{m}\ ]$	Length of the mean aerodynamic chord
$\bar{c}'$	$[\ -\ ]$	Relative length of the mean aerodynamic chord
$\bar{V}'$	$[\ -\ ]$	Modified volume coefficient
Δp	$[\ \text{N/m}^2\ ]$	Pressure difference

Nomenclature

Λ	$[\ -\ ]$	Aspect ratio
λ	$[\ -\ ]$	Taper ratio
ν	$[\ \circ\ ]$	Dihedral
σ_1	$[\ \text{N/m}^2\ ]$	Axial stress at the ellipse half-axis x
σ_2	$[\ \text{N/m}^2\ ]$	Axial stress at the small ellipse half-axis y
σ_A	$[\ \text{N/m}^2\ ]$	Dimensioning axial stress
τ	$[\ \text{N/m}^2\ ]$	Shear stress
φ	$[\ \circ\ ]$	Sweep
A	$[\ \text{m}^2\ ]$	Area
b	$[\ \text{m}\ ]$	Wingspan
C_L	$[\ -\ ]$	Lift coefficient
C_M	$[\ -\ ]$	Pitching moment coefficient
$C_{D,0}$	$[\ -\ ]$	Zero-lift drag coefficient
C_D	$[\ -\ ]$	Drag coefficient
$C_{L,cruise}$	$[\ -\ ]$	Lift coefficient in cruise
$C_{L,mD}$	$[\ -\ ]$	Lift coefficient for minimum drag
d_f	$[\ \text{m}\ ]$	Outside diameter fuselage
$D_{i,A320}$	$[\ \text{N}\ ]$	Induced drag of the A320-200
$D_{i,box}$	$[\ \text{N}\ ]$	Induced drag of the boxwing
$D_{i,ref2}$	$[\ \text{N}\ ]$	Induced drag of the second reference aircraft
E_{opt}	$[\ -\ ]$	Optimal glide ratio
h	$[\ \text{m}\ ]$	Horizontal distance of the leading edge of the front wing to the center of gravity
h/b	$[\ -\ ]$	Height-To-Span Ratio
h_0	$[\ -\ ]$	Aerodynamic center
l	$[\ \text{m}\ ]$	Horizontal distance of the aft wing to the center of gravity
l'	$[\ \text{m}\ ]$	Horizontal distance of the wings
l_{root}	$[\ \text{m}\ ]$	Length of the wing root

Nomenclature

l_{tip}	[m]	Length of the wing tip
M_t	[Nm]	Torsional moment
Ma	[−]	Mach number
Ma_{cruise}	[−]	Mach number in cruise
MAC	[m]	Mean Aerodynamic Chord
s	[−]	Relative reference area of the wing
S	[m^2]	Surface
S_{proj}	[m^2]	Projected area in a vertical plane
T/W	[−]	Thrust-to-weight ratio
t_W	[m]	Wall thickness
U_C	[m]	Circle perimeter
U_E	[m]	Ellipse perimeter
W/S	[kg/m^2]	Wing loading
x	[m]	Half-axis of the ellipse
x_{CG}	[m]	x-Position of the center of gravity
x_{LEMAC}	[m]	x-Position of the Leading Edge of the Mean Aerodynamic Chord
y	[m]	Small half-axis of the ellipse

1 Introduction

Worldwide air travel is expected to grow continually for the foreseeable future. This growth can be observed globally, especially in the Asian market [47]. While demand for affordable air travel keeps rising, there is increasing concern about the environmental implications of this growth. To address these concerns, a number of institutions, including the European Union, IATA and ICAO have set ambitious goals to limit the impact aviation has on earth's climate and environment[16]. These goals include the commitment to cap the aviation related net CO_2 emissions from 2020 onwards [38]. Another problem associated with this continuous growth in aviation is the increasing number of airports at their capacity limits [25]. To deal with these challenges, innovative solutions are needed. The AixBox One (AB-One), as shown in figure 1.1, is an aircraft concept developed to satisfy future demands for an ultra-efficient, low emissions aircraft. It can easily meet the goals issued by NASA and DLR [52, 12] to design a highly efficient aircraft. The main objective of the NASA/DLR Design Challenge is to reduce energy consumption by 60 %, compared to the best in class reference aircraft of 2005. Short to medium range missions make up for the biggest portion of the aviation industry [1]. Hence, this mission profile was chosen to maximize the potential impact of this concept. To evaluate AB-One's performance, the Airbus A320-200 is chosen as reference aircraft, as it fulfills mostly the same mission requirements and has a similar mass. All referenced data is obtained from the CeRAS database [68]. One additional constraint of the challenge is that the designed aircraft has to fly at the same cruise Mach number as the reference aircraft.
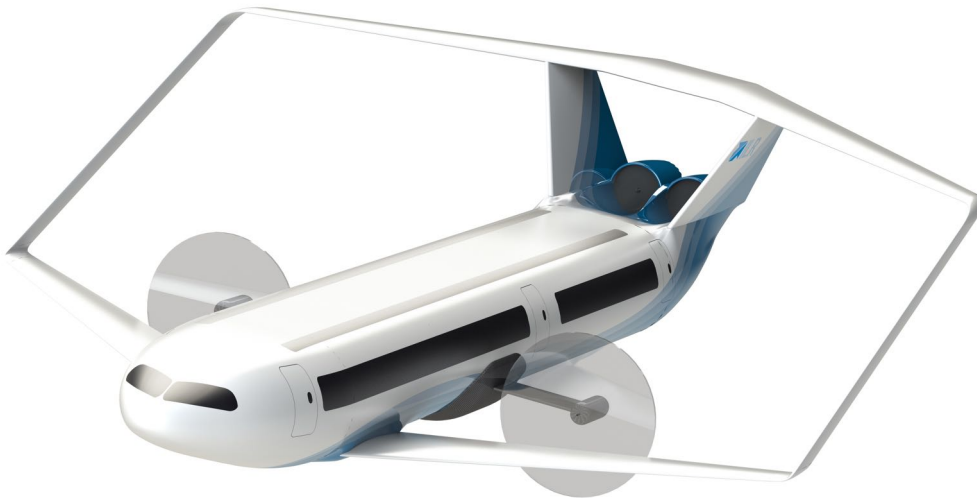
Figure 1.1: AixBox One

The first difference between AB-One and the A320-200 is their maximum range. Statistical evaluations have shown that more than 90 % of all short and medium haul flights cover a flight distance below 1650 NM [44]. Present aircraft are highly oversized, which scales up the structural weight unnecessarily. With the reduced design range of 1800 NM, AB-One is able to handle practically all missions covered by the A320-200. In any particular case, when higher range is demanded, it is possible to reduce payload and increase fuel mass, compare with figure 8.1.

Chapter 1. Introduction

Second, forecasts of Airbus [1] and DLR [4] indicate a strong growth of passenger volume for the next decades. Since many airports are already touching their departure capacity limit [31], larger aircraft are a possible solution to meet these high demands. From these predictions it can be concluded that a growth of 70 % until 2045, meaning approximately 100 passengers more compared to the A320-200, will be reasonable. In order to reach this passenger capacity without making AB-One unnecessarily longer, a double-bubble configuration (DB) is chosen. This corresponds to the juxtaposition of two conventional cylindric fuselages, which accommodates 264 passengers. Furthermore, the double-bubble fuselage also helps to generate additional lift, which allows for a smaller wing area, reducing drag.

This analysis of the evolution of air traffic, combined with the constraints given by the Design Challenge lead to the following main requirements for AB-One.

Table 1.1: Main requirements for AB-One

	AixBox One	**Origin of constraint**
Energy savings [%]	60	Design Challenge
Cruise Mach number	0.78	Design Challenge
Design Range [NM]	1800	Market analysis
Passengers	264	Market analysis

In order to reach these goals, several decisions concerning the configuration of AB-One have to be made, which will be elaborated on hereafter.

First of all, a boxwing configuration is chosen for the wing. It allows to reduce the induced drag of the aircraft, especially during takeoff and landing. As AixBox One is a short and medium haul aircraft, the proportion of takeoff and landing procedures are relatively high compared to cruise, which allows for a maximum benefit of this configuration. In a boxwing, one wing is replaced by two, which reduces the induced drag. This phenomenon and its consequences on the fuel consumption of the aircraft will be explained in chapter 4. A V-shaped tailplane is designed to bear the aft wing and the rudders, as it reinforces the structure of the boxwing, compare with chapter 4.2.

Second, one of the greatest disadvantages of conventional aircraft are the engines, being oversized for takeoff and climb, as the rolling and aerodynamic drag must be overcome. During cruise flight, however, significantly less thrust is required. For the A320-200, the thrust needed during cruise flight amounts to roughly 20 % of the thrust needed for takeoff, which leaves room for optimization. For AB-One, the conventional engine configuration is replaced by two propulsion systems, the AixBox Booster (ABB) and the main engines. ABB is a support device, i.e. an autonomous aircraft by itself, only designed to support takeoff and climb. It provides additional thrust during these thrust intensive flight segments. When the desired flight level is reached, ABB is detached from AB-One and the main engines solely provide propulsion for the remainder of the flight. Therefore, the main engines are downsized appropriately, reducing mass and fuel burn. They are mounted on the back of the fuselage and ingest the boundary layer to allow for further fuel savings. The main engines' position also reduces noise emission, as the fuselage is shielding the engines from underneath. The main engine is discussed in chapter 5.

Next, to further reduce structural weight and aerodynamic drag, the landing gear is replaced by a ground based landing system. It also significantly reduces rolling resistance and adds a supplementary propulsion force to the aircraft [50]. The concept works as follows. During takeoff, like a conventional aircraft, AB-One is accelerated by the main engines. These are supported by the magnetic sledge and ABB until takeoff speed is reached. For landing, the sledge is accelerated until the speed of the approaching aircraft is met. As soon as all relevant parameters are synchronized, AB-One is attached to the sledge by a self-locking system. This system reduces noise emission and the maximum takeoff

weight (MTOW) is reduced by $3 - 4\%$, as the landing gear is substituted with force transmission points. The difficulties coming along with this technology are discussed in chapter 6.

Finally, since entry into service is 2045, additional structural weight reduction through utilization of composite materials and their anisotropic properties is also taken into account. In order to enhance passenger experience, advanced transparent composite materials are used to drastically increase window size without adding a weight penalty [6]. Figure 1.2 depicts AB-One with all its components.
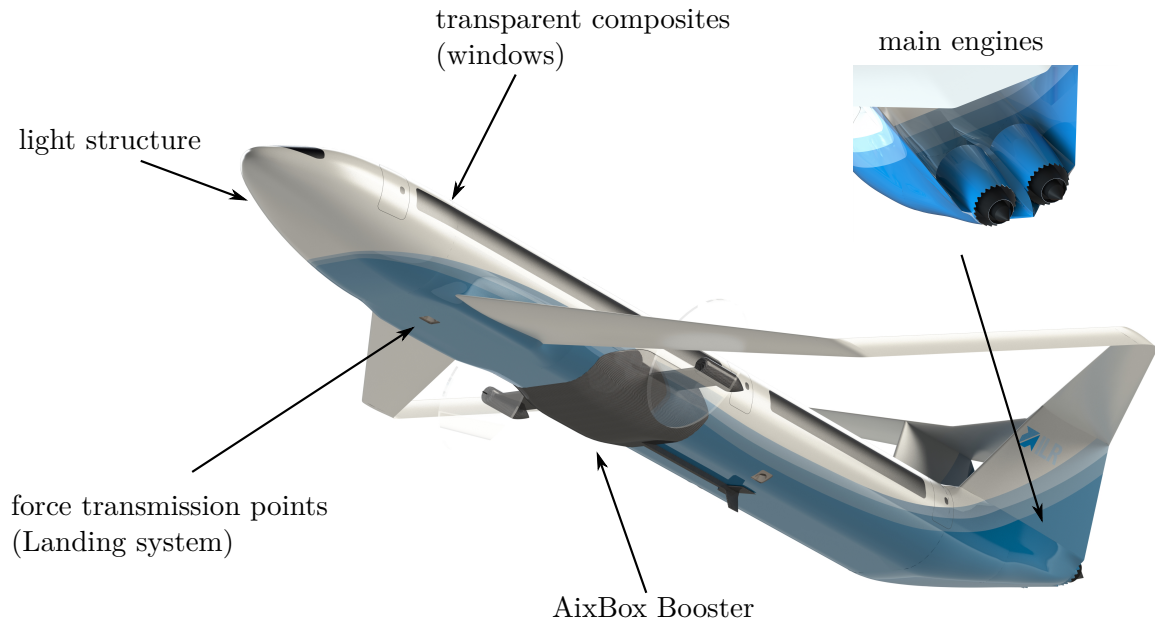
Figure 1.2: AixBox One components

For the boxwing, literature from Scholz, Schiktanz, Jemitola and Zohlandt is studied, who made profound investigation in this field of study. Also, the development of the D8 by Drela et al. gave many valuable inspirations for the design. Regarding the development of the ABB, the battery road map by the Fraunhofer ISI is of particular importance.

2 Initial Sizing

The first step of the preliminary aircraft design is the initial sizing. It allows to generate constraints for the thrust-to-weight ratio (T/W) and the wing loading (W/S) for the different flight segments and serves as input for the wing and engine design. The starting point is given by the Top Level Aircraft Requirements (TLARs). The TLARs represent the specific requirements of an aircraft usually set by airlines and manufacturers, see table 2.1. In this case, the TLARs are partially defined by the requirements of the Design Challenge.

With these requirements, the design diagram of the initial sizing [66] can be derived in accordance with the work done by [56, 61, 41]. As it can be seen in figure 2.1, AB-One's diagram has some major differences compared to that of a typical A320-200. A high efficiency factor resulting from the boxwing concept improves the lift distribution, see chapter 4, and increases the glide ratio. Without having a landing gear, drag during climb and approach is reduced. Less drag and a higher glide ratio imply less required thrust, resulting in a higher efficiency. Due to the detached ABB, a considerable weight saving for the cruise and landing can be achieved which allows for higher maximum W/S. Lastly, with the main engines being optimized for cruise, a remarkable improvement in cruise efficiency can be achieved.

Table 2.1: Top Level Aircraft Requirements for AixBox One

	AixBox One	**A320-200**
Energy savings [%]	60	
Cruise mach number	0.78	0.78
Design Range [NM]	1800	2500
Passengers	264	150
Design Payload [kg]	26186	17000
Maximum Payload [kg]	29602	20000
Cargo [kg]	8881	6000
Flight altitude [ft]	35000	35000
Balanced Field Length [m]	max. 2100	2100
Landing length [m]	max. 1600	1600
Number of engines	2 plus ABB	2

To guarantee enough thrust in the case of a go-around, additional constraints are established for the engines, see chapter 5.

(a) A320-200

(b) AixBox One
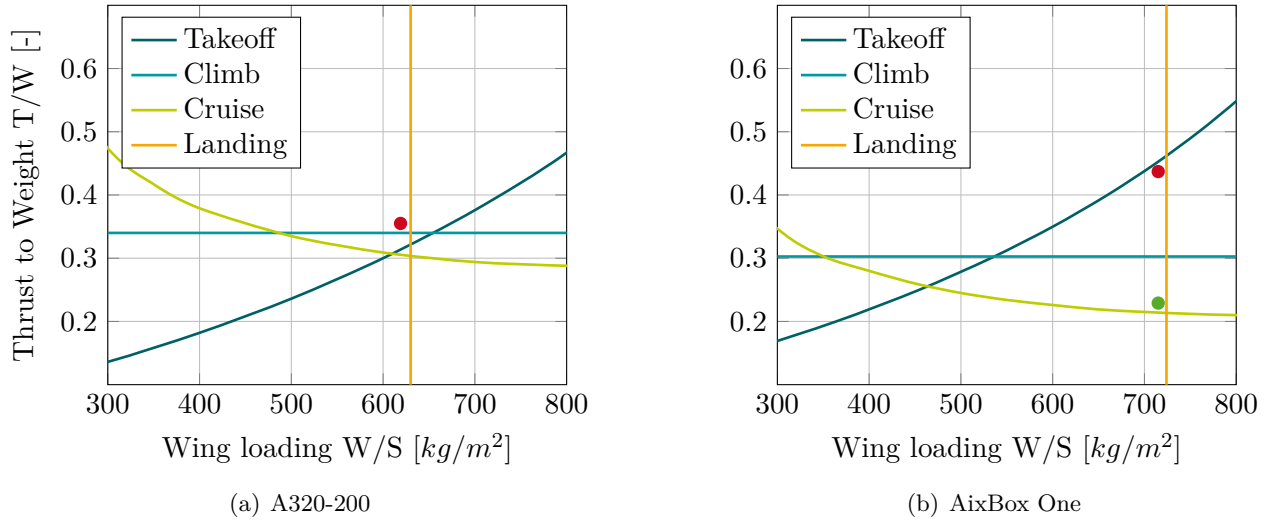
Figure 2.1: Initial sizing diagram

Usually, the design point is chosen in the allowed area above the curves at highest possible W/S and lowest T/W. At this point, the aircraft has sufficient thrust for all flight segments with a relatively low wing area for less drag and weight (compare with A320-200 in figure 2.1(a)). However, with the use of ABB, not only one design point for the aircraft can be set, but two. The first point represents takeoff and climb (see red point in figure 2.1(b)), whereas the second point stands for cruise and landing (see green point in figure 2.1(b)). This makes a higher W/S possible, which decreases the wing area and the structural weight. During takeoff and climbing, the booster provides the aircraft with high thrust and thus, high acceleration. The design point is located slightly below the takeoff curve, because the magnetic sledge is supporting the aircraft with additional energy. The second point can be placed far below the takeoff design point, since the thrust requirements for cruise are notably lower. As a result, the engines can be optimized for cruise and therefore, have a higher efficiency.

The $C_{L,cruise}$ calculated in chapter 4.3 is not further limiting the wing loading. Thus, the following design points are chosen for the AB-One:

Table 2.2: Design points

	$T/W[-]$	$W/S[kg/m^2]$
Takeoff, Climb	**0.45**	**720**
Cruise, Approach	**0.22**	**720**

3 Fuselage

The weight-optimal fuselage cross section is usually circular. However, nowadays two further configurations are widely investigated: The double-bubble fuselage and the Blended Wing Body (BWB). A broader body is producing additional, centered lift so that the wings' area and weight can be further reduced for the DB and BWB [58]. With a lower wetted area referenced to the same fuselage volume, they produce less friction drag per passenger [49]. However, the main drawbacks of the BWB are the need for artificial stability and having high roll accelerations at the tip of the wing reducing passenger comfort. Hence, for this design the DB is regarded as the best solution since it combines the advantages of a wider body without having too high roll accelerations.

To assess the optimum fuselage cross section structure, two different cases are discussed: A simple elliptical fuselage and a fuselage with struts in the middle, see figure 3.1.

(a) Elliptic fuselage

(b) Fuselage with struts reinforcement
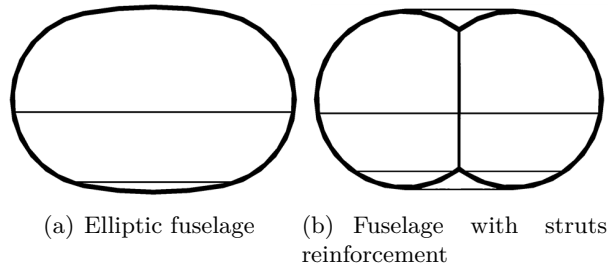
Figure 3.1: Comparison of two different fuselage geometries

The struts reinforce the structure since the pressure distribution for an elliptical cross section is inhomogeneous in contrast to a circular one. As a simplification for the calculation of the fuselage with struts, it is assumed that there are two circular segments next to each other, see figure 3.2(b).

(a) Elliptic sketch

(b) Circular sketch

(c) Elliptic section

(d) Circular section
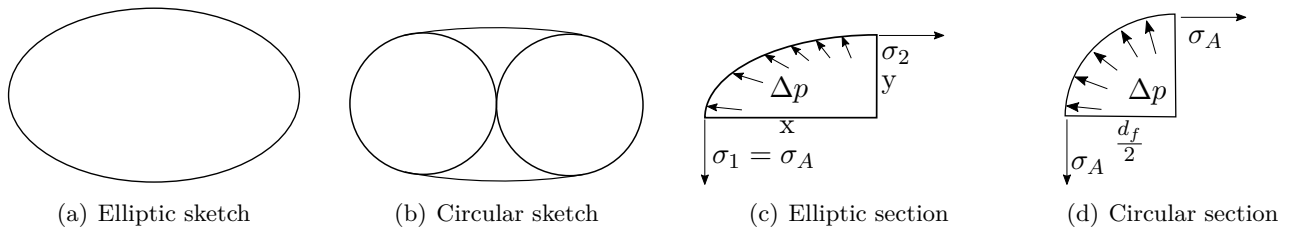
Figure 3.2: Sketches of the different fuselage geometries

With Barlow's formula [15]

$$t_W = \frac{d_f \cdot \Delta p}{2 \cdot \sigma_A} \tag{3.1}$$

the required wall-thickness t_W for a given pressure difference Δp can be calculated. For an elliptic cross section, the dimensioning normal stress is σ_1, assuming a constant thickness along the circle, see 3.2(c). The circular section in 3.2(d) with radius $\frac{d_f}{2}$ has constant normal stress σ_A.

$$\frac{m_C}{m_E} = \frac{\rho_C \cdot V_C}{\rho_E \cdot V_E} = \frac{t_C \cdot U_C}{t_E \cdot U_E} \tag{3.2}$$

With Barlow's formula for t_W, the perimeter definitions of a circle U_C and an ellipse U_E, and assuming the length and pressure difference are the same for the two shapes, the following relation can be established:

$$\frac{m_C}{m_E} = \frac{t_C \cdot U_C}{t_E \cdot U_E} = \frac{d_f \cdot [2 \cdot \pi \cdot \frac{d_f}{2}]}{2 \cdot x \cdot [\pi \cdot (x + y)]} \tag{3.3}$$

Assuming that the half-axis of the ellipse x equals the radius of the circle $\frac{d_f}{2}$ and $y = \frac{x}{2}$, the ratio of the masses is $\frac{m_C}{m_E} = \frac{2}{3}$, meaning the mass of the ellipse with struts for reinforcement will be around 33 % lower.

The final fuselage design is shown in figure 3.3(a). Incorporating a twin-aisle cabin, faster turnaround can be achieved, which reduces direct operating costs [24]. With and an overall aircraft length of 41.17 m, it is possible to carry 240 passengers in economy class with a seat pitch of 0.78 m and 24 passengers in business class with a pitch of 1.52 m compare with picture 3.3(b). The cabin is able to accommodate 10 passengers per row, increasing the number of passengers by 114 in a two class configuration, compared to the A320-200. To take advantage of the broad cockpit, one galley can be placed next to the cockpit. Three exits of Type A are sufficient for emergency egress [19], the middle exits are positioned at a safe distance from the booster and the wings. Sophisticated, transparent fiber reinforced thermoplastics [6] will be used to have continuous panoramic windows for creating a unique flying experience. Besides that, AB-One can hold two rows of 12 LD3-45 cargo containers. As a medium-haul aircraft, low cost airlines will have interest in carrying as many passengers as possible without a business class. Therefore, picture 3.3(b) also shows an alternative cabin layout with 330 passengers, still satisfying all requirements concerning the emergency egress, number of galleys and lavatories. To stay within MTOW, the cargo ratio needs to be decreased.
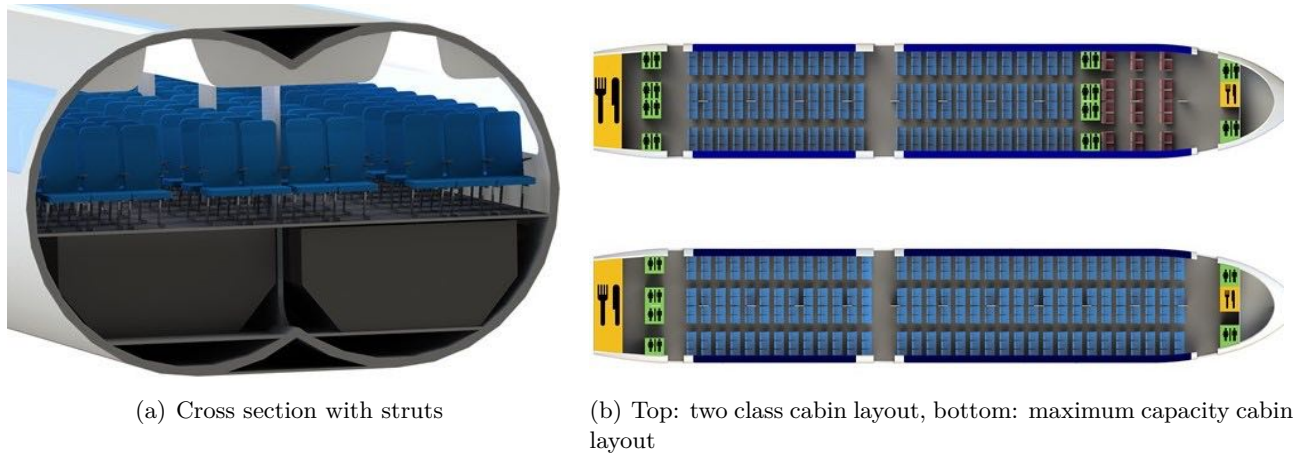

(a) Cross section with struts

(b) Top: two class cabin layout, bottom: maximum capacity cabin layout

Figure 3.3: Fuselage cross section and cabin layouts

4 Boxwing

A boxwing is considered best to reduce the induced drag for a given span [55, 23, 53, 79]. During cruise, induced drag is about 35 % of total drag and goes up to 90 % during takeoff and landing [43]. Especially for short-haul flights, the ratio of approach and landing procedures compared to the whole flight is high. This is even intensified by the reduced operating range of the AB-One as mentioned in chapter 1. Therefore, using a boxwing with its minimized induced drag has a significant impact on the total drag of the aircraft. For a given span, the boxwing can achieve the highest efficiency factor [79, 55] which is decisive for the induced drag. Considering an ideal boxwing, where both wings carry half of the lift of a conventional reference aircraft and have the same geometry characteristics, the induced drag can be halved [63].

All final wing parameters can be found in A.1. A high wing loading from the initial sizing results in a small wing area, which is distributed equally on both wings. The aspect ratio is one of the free variables that can be selected. High values lead to a low induced drag on the one hand but increase the root bending moment and therefore, the MTOW. Especially for a boxwing, where the given wing area is split into two wings, the wing chord is very short which can cause structural issues. Following a sensitivity analysis in [83], where these effects are considered, a lower total aspect ratio of 6.25, compared to the A320-200, is chosen as an optimum. This leads to a wingspan of $26.43\,m$ that is slightly larger than the limits for category B which is set at $15\,m$ - $24\,m$ in the ICAO Aerodrome reference code [40]. A further reduction of the wingspan could potentially reduce airport handling fees, but is accompanied by an even lower aspect ratio and therefore higher induced drag. Since the main purpose of this concept is to reduce energy consumption, a span of $26.43\,m$ is chosen.

The taper ratio is set to 0.33 which is a trade-off between having a low induced drag, a low bending moment and enough space for fuel, flaps and the aileron in the outer part of the wing [41]. The sweep has a large impact on the aerodynamic performance and stability. To enhance stability by increasing the horizontal gap between both wings, a high sweep is necessary. Conversely, too high values lead to cross flows with flow separation and flutter effects especially for the forward swept wing [57]. 34° for the fore wing and -28° for the aft wing are chosen as sweep in accordance with the stability evaluation of chapter 4.1 and the optimum analysis in [53].

4.1 Stability

The longitudinal stability is one of the main concerns of the boxwing [64], which is why a stability analysis is performed. To calculate the acceptable range of the center of gravity (CG), an approach according to [62] is chosen, compare with figure 4.1.
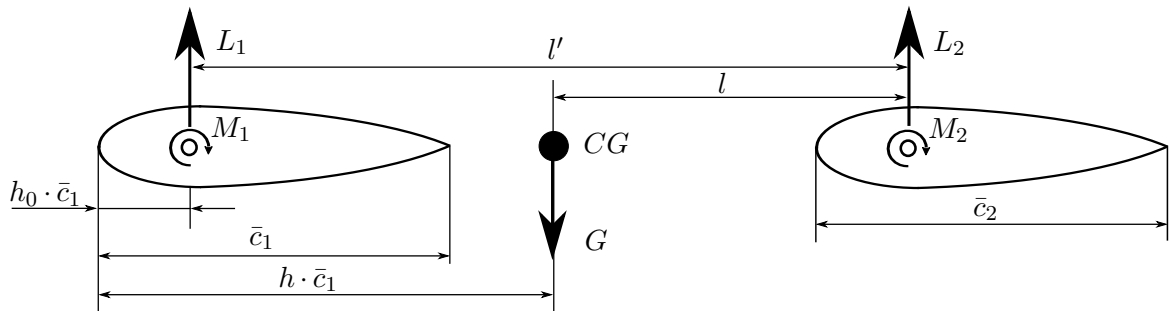

Figure 4.1: Sketch of the MAC's of the boxwing for stability analysis [62]

Figure 4.1 depicts the cross sections of the MAC ($\bar{c}$) with lift and moment of both wings. Assuming drag is negligible for the momentum equilibrium, they can be simplified to be at the same height. The indices 1 and 2 indicate the fore and aft wing of the boxwing. From the equilibrium of moments, the conditions in table 4.1 can be derived [62].

Table 4.1: Controllability and stability conditions

Condition	General expression	Derived boxwing condition
Stability	$\frac{dC_{M,CG}}{dC_L} < 0$	$h < h_0 + \frac{dC_{L,2}}{dC_L} \cdot \frac{\bar{V}'}{c'_1}$
Trimability	$(C_{M,CG})_{C_L=0} > 0$	$h > h_0 + \frac{C_{L,2} \cdot \bar{V}'}{C_L \cdot c'_1} + \frac{C_{M,1}}{C_L} \cdot s_1 + \frac{C_{M,2}}{C_L} \cdot s_2 \cdot \frac{\bar{c}_2}{\bar{c}_1}$
Controllability	$C_{M,CG} > 0$	$C_{M,1} \cdot c'_1 \cdot s_1 + C_{M,2} \cdot c'_2 \cdot s_2 - (C_{L,2})_{C_L=0} \cdot \bar{V}' > 0$

All values are calculated in accordance with [64] and can be found in Appendix A. Since the boxwing does not have a horizontal tail plane causing a nose up moment, the wings need to trim the aircraft by themselves. To guarantee a trimmed and controllable aircraft, the condition $C_{L1} > C_{L2}$ is fulfilled with a greater incidence angle of the fore wing. However, with a larger gradient of the lift coefficient $\frac{dC_L}{d\alpha}$ of the aft wing, the aircraft is able to create a negative pitching moment for higher angles of attack to enable longitudinal stability. This relation is illustrated in figure 4.2(a). It shows the general course of the lift coefficient for both wings for different angles of attack. To trim the aircraft in cruise, the fore wing needs a higher lift coefficient since its lever arm to the CG is shorter compared to the aft wing and the zero moment of the wings needs to be balanced out. The trim condition is indicated with red crosses. Due to different sweep angles, the aft wing has a higher gradient of the lift coefficient. If the pitch angle increases, the difference between both lift coefficients decreases. This means, the aft wing generates a higher moment resulting from a higher lever arm. The fore wing stalls first, which ensures that the aircraft is stabilized by a nose-down moment. This is supported by the downwash of the fore wing, which reduces the effective angle of attack of the aft wing and therefore, causes the aft wing to stall later [83].
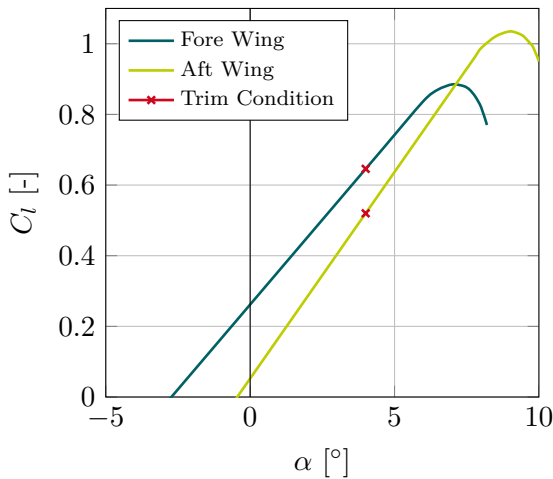
(a) Lift coefficient of the fore and aft wing
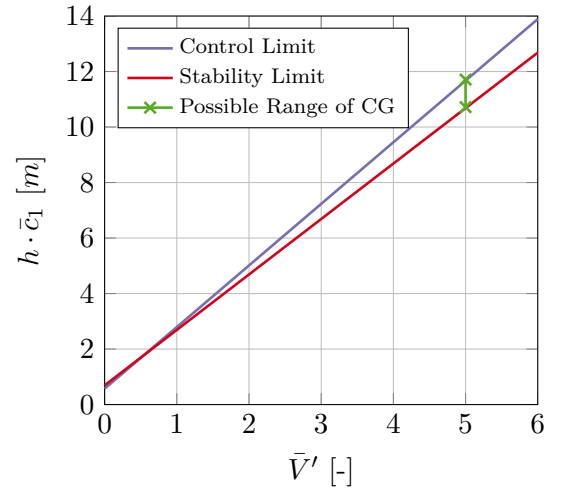
(b) Possible range of the CG

Figure 4.2: Stability and controllability analysis of the boxwing

To enhance the controllability, the lower part of the cockpit section of the aircraft is shaped upwards to get an additional positive pitching moment [13] and the inner part of the aft wing between the V-Tail

is straightened to use it as elevator. For the possible range of the CG, the determining parameter is the modified volume coefficient $\bar{V}' = \frac{l' \cdot s_2}{\bar{c}}$, see figure 4.2(b). As the distance l' between both wings increases, so does the volume coefficient and consequently, the possible range of the CG denoted by the minimum and maximum $h \cdot \bar{c}_1$. Thus, a high volume coefficient is chosen for the boxwing, resulting in a range of the CG from $21.5\,m$ to $22.71\,m$.

The condition for lateral stability for the roll axis reads $C_{l,\beta} < 0$. A dihedral of $4°$ and the high backward sweep ensure the stability for the fore wing. For the aft wing, no dihedral is used as it can cause structural problems at the connection point with the empennage [62]. A forward swept wing creates an unstable roll moment, while a high-wing configuration has a stable roll moment component. Considering all these factors, roll stability can be deducted. The lateral stability analysis for the yawing axis is performed in the next section.

4.2 Empennage

For the empennage, a V-Tail is selected. Relative lateral displacement of the two wings can occur at sideslip angles. The V-Tail can bear the wing loads best [8] and is therefore used to ensure structural stability of the aft wing. The parameters of the V-Tail are tabulated in Appendix A.3. A forward sweep of -33° supports the longitudinal stability, as it pushes the wings more to the front and helps to adjust the possible range of the CG. The empennage area is sized due to the lateral stability conditions for the yaw axis $C_{n,\beta} > 0$ and $C_n > 0$. In accordance with [35], the derivatives for the components of the wings, fuselage and V-Tail can be calculated, compare with A.4. The forward swept wing and the fuselage have a destabilizing and the backward swept wing a stabilizing derivative. The tail area is sized to guarantee a stable flight state with one engine inoperative. Having two engines centered on the wing and an ABB that can be shut off and detached in the case of an emergency, only a small yawing moment needs to be balanced out. A vertical area of $14\,m^2$ for each fin is calculated for controllability and therefore a total tailplane of approximately $40\,m^2$ is needed due to the dihedral of 45° of the V-Tail. Having the wing on top of the V-Tail increases the efficiency of the V-Tail as the wing acts as an end plate [10]. For placing the wing on the V-Tail, the tip length of the empennage has to match the chord length of the wing at the connection point.

4.3 Aerodynamic Performance and Drag

The main aerodynamic improvement of the boxwing is related to the higher Oswald factor compared to a conventional wing. To quantify the reduction of the induced drag, the ratio of the efficiency factors e_{box}/e_{ref} are calculated with the method according to [59], which is evaluated to be the most accurate [63]:

$$\frac{D_{i,box}}{D_{i,ref}} = \frac{0.44 + 0.9594 \cdot (h/b)_{box}}{0.44 + 2.219 \cdot (h/b)_{box}} = \frac{e_{ref}}{e_{box}} \tag{4.1}$$

The higher the gap-to-span ratio h/b of the two wings, the better the efficiency factors. The gap-to-span ratio is set to 0.25 to obtain a high efficiency factor of the boxwing [43], but to keep the risk of flutter phenomena fairly low [45, 65]. With $h/b = 0.25$, an efficiency factor of 1.25 can be achieved. AB-One has different wing characteristics than the A320-200. Since the efficiency factor is referenced to an aircraft with the same aspect ratio and wing area [62], a scaled A320-200 as second reference aircraft (ref2) with the same wing characteristics as the boxwing is generated with MICADO [36]. The vortex lattice method is used to determine the Oswald factor and calculate an induced drag of $D_{i,ref2} = 15.8\,kN$ for the reference aircraft, and $D_{i,A320} = 15.5\,kN$ for the A320-200. The factor

is slightly higher for the second reference aircraft because the wing and span is downsized to the values of AB-One. With the efficiency factor, the induced drag for the boxwing can be derived to $D_{i,box} = 10.74\,kN$. Doing so, a drag penalty is added [62], since both wings do not carry the same amount of lift due to stability reasons and therefore differ from an ideal configuration, see chapter 4.1. Considering the different wing areas of the boxwing and the A320-200, a final improvement of $31.0\,\%$ can be achieved for cruise, which is $10.8\,\%$ of the total drag. In takeoff conditions, this amount even increases to a value of $27.4\,\%$.

Having a closer look at the aerodynamics, the relations in table 4.2 can be found.

Table 4.2: Aerodynamical values of AixBox One and the A320-200

Parameter	AixBox One	A320-200
$C_{L,mD}$	0.58	0.54
$C_{L,cruise}$	0.63	0.60
E_{opt}	18.5	17.6
$C_{D,0}$	0.0165	0.0192

The optimal glide ratio for boxwings has typical values around 20, see [65]. However, due to the decrease of the aspect ratio for structural reasons, a lower glide ratio is reasonable. To compare different configurations, three polars are calculated for Ma_{cruise} with an exemplary symmetric profile. To calculate the zero-lift drag coefficient $C_{D,0}$ in cruise, OpenVSP is used [27]. The reasons for the low value compared to the A320-200 are the following. The wing area is significantly smaller because of the high wing loading. Also the engines are mounted on top of the fuselage, so no pylons and significantly smaller nacelles are needed. Further, there is no horizontal tailplane. The fuselage has a bigger wetted area, but is included in the total drag with a lower weighting [67]. Moreover, a riblet surface is used to reduce the skin friction [7].

Boxwings typically have a higher lift coefficient at minimum drag than the referring conventional aircraft's wing [62]. To increase the lift coefficient during cruise for a constant total lift, the boxwing aircraft needs to fly higher for lower air density. However, since AB-One has a very high wing loading, the wing area is very small which already requires a higher lift coefficient. Hence, AB-One can fly on the same flight level as the A320-200. The increased induced drag for a higher C_L is hereby outweighed by the small C_{D0} of the wing.
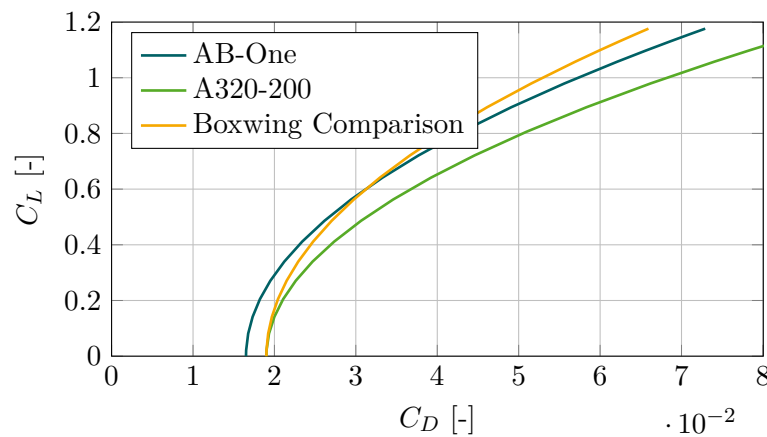

Figure 4.3: Lilienthal polar

To evaluate the performance of AB-One, a simplified Lilienthal Polar with a symmetric airfoil is generated, see figure 4.3. The green curve shows the polar of the A320-200. The yellow curve indicates a polar of a boxwing aircraft with the same total wing area, aspect ratio and zero-lift drag like the A320-200. It can be noted that the curve has a higher slope due to the high glide ratio, meaning that for the same lift coefficient, less drag is produced. AB-One with its lower aspect ratio has a slightly higher slope than the A320-200 and a low zero-lift drag. Hence, it still generates less drag than the A320-200 and until a lift coefficient of 0.6 even a lower drag compared to a boxwing with the same wing area and zero-lift drag like the A320-200.

4.4 Structure and Airfoil

The airfoil of the boxwing has a complete different composition than the airfoil of a conventional aircraft. A higher incidence angle is incorporated for the front wing to ensure that the front wing will stall first for longitudinal stability, see chapter 4.1. As mentioned in [53], the bending axis for boxwings is inclined, see figure 4.4.

Figure 4.4: Airfoil structure [53]

Since the stress reaches its maximum in the point the furthest away from the neutral axis, the structure needs to be stiffened in the upper part of the leading edge and the lower part of the trailing edge. The structure increases the volume of the inner wing part to carry more fuel. However, since the total volume of the boxwing is halved, additional tanks are necessary in the fuselage . They are placed in the void between the pressurized cabin structure and the outer skin of the fuselage, see figure 4.5.
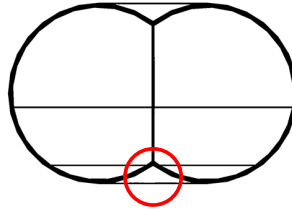
Figure 4.5: Positioning of additional tanks

The thickness-to-chord ratio t/c effects aerodynamics as well as structure. A low value reduces pressure drag, while a high value reduces structural weight. In accordance with [53], an optimum t/c of 0.1 is chosen. Taking into account the low chord length of a boxwing, which is nearly halved for AB-One. Designing a low-weight structure can be a challenge because of the low resulting thickness. Bredt's formula [9] for closed, thin profiles reads

$$t_W = \frac{M_t}{2 \cdot A \cdot \tau} \tag{4.2}$$

Assuming constant t/c the halved chord length of AB-One's wings implies a halved wing thickness. The enclosed areas A of both wings then add up to about a half of the conventional wing's area. Hence the wall thickness has to be doubled, which also incorporates doubling the weight. This is valid for constant torsional as well as constant bending moments.

As the wings are connected, torsional movement is resisted by the bending stiffness of the other wing. Concerning the bending moment, a nose down twist can be observed at the backwards swept wing's tip, while the forward swept wing shows a nose up twist. A boxwing configuration counteracts these movements due to the connection of the wingtips. However these joints have to carry substantial loads. To determine bending loads at the root on a preliminary basis, a simplified calculation of the bending moment (BM) along the wing is performed with Stab2D [37]. The conventional wing is simplified as an encastred beam with a linear section load, compare with figure 4.6(a). For this configuration, a maximum BM at the wing root of $6743\,Nm$ is calculated (see 4.6(b)). Figures 4.6(c) and 4.6(d) show the same procedure with a boxwing, pictured as three beams connected to each other. Since every wing of the boxwing carries nearly half of the lift of the conventional wing, the loads are halved. The geometry of the beams are chosen according to the span of the A320-200 and AB-One. The maximum BM of the boxwing configuration is reduced to $1412\,Nm$, less than a quarter of the reference value. It can be concluded that for the first design step, no severe structural problems are expected.

| (a) Loads wing | (b) BM wing | (c) Loads boxwing | (d) BM boxwing |
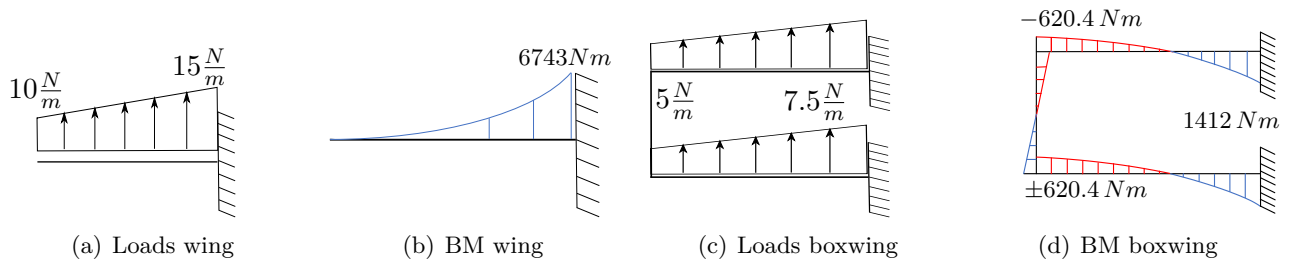
Figure 4.6: Comparison of the bending moment for a wing and a boxwing

4.5 High-Lift Devices & Control Surfaces
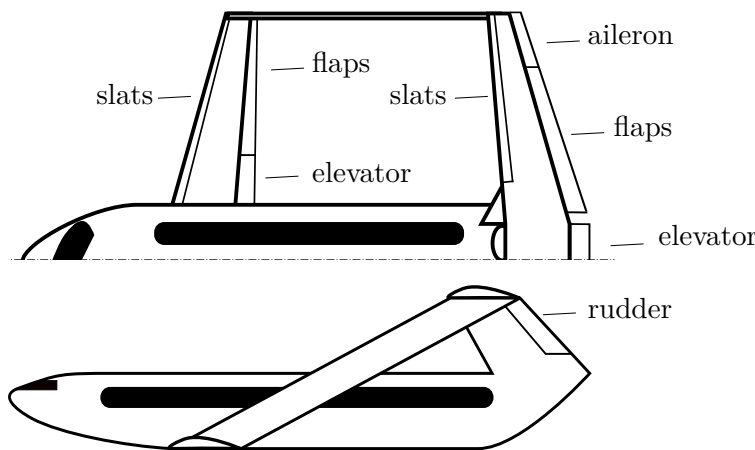
Figure 4.7: Positioning of control surfaces and highlift devices

Because of high speed at liftoff, the required lift coefficient $C_{L,T/O}$ of 2.08 for AB-One during takeoff, including a safety factor of 1.3, is slightly smaller compared to the A320-200. This high speed comes from the high acceleration, which is limited to $0.5\,g$, in order not to exceed passenger comfort limits [33]. This acceleration is made possible by combined use of the engines, ABB and the sledge. For landing, high-lift devices are required in order to slow down the plane enough, before it is caught by the magnetic sledge. As required C_L values are higher for landing than takeoff, landing is the dimensioning case. Therefore, dropped hinge flaps are installed at the trailing edge of both wings and slats at the leading edge. It is then possible to increase $C_{L,max}$ to values between 2.5 and 2.9 for landing and 2.0 to 2.2 for takeoff [70]. In order to get the required moment induced by the control surfaces with a fixed area, the aim is to get the highest lever arm. This explains the placement of the control surfaces in figure 4.7. The shape parameters for the three control surfaces according to [70] can be found in table 4.3.

Table 4.3: Shape parameters for the control surfaces

	Rudder	Aileron	Elevator
Span	2.7	3.25	4.02
MAC	1.62	1.35	1.4

5 Main Engines

5.1 Layout

One major strategy to enhance fuel efficiency in jet engines is increasing the bypass ratio (BPR). Nowadays BPRs of 12 are common, whereas values as high as 18 are expected for the next engine generation [75]. While they provide a benefit during takeoff, their large fans increase the overall aircraft weight as well as nacelle drag, which is especially significant during cruise flight. Since AB-One is equipped with ABB, the takeoff benefit of a high BPR engine is not relevant. AB-One comes with two turbofan engines, that are mounted on top of the fuselage's rear section and fit in between the V-Tail, see figure 5.1. The fuselage's rear geometry is designed for optimal airflow into and around the engines. With these two engines, AB-One complies with the certification requirements concerning in case of one engine inoperative. Supplementary, nacelle reinforcements are implemented to prevent separated blades from damaging the neighbouring engine. Due to the engine location, the fuselage boundary layer is ingested which leads to a significant improvement of aerodynamic drag [74]. As a result of using boundary layer ingestion technology (BLI), engine inlet distortion effects must be taken into account. These effects can be mitigated by using a non-axisymmetric stator geometry [30]. Additionally, the engine placement results in a reduction of nacelle and interference drag as well as noise. Generally speaking, the engine location is unfavourable for maintenance due to poor accessibility. However, the main engines require less frequent maintenance because of the thrust support from ABB during takeoff. Normally, the aircraft's engines operate at peak power during takeoff, causing higher wear. Moreover, they are protected from runway dirt, debris and bird strike, since they are located on top of the fuselage. Considering the afore-mentioned aspects, AB-One's engines achieve a longer operational lifetime, reducing operational costs for airlines.

5.2 Engine Core
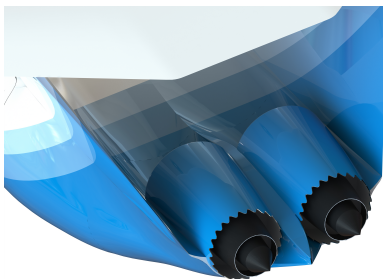
Figure 5.1: Position of the main engines

In order to reduce power required by the compressor, an intercooler is added to the engine core. Due to smaller amounts of required compressor power, the engine core and therefore the engine weight can be decreased. However, the reduction of compressor exit temperature leads to a reduction in thermal efficiency. Therefore, a recuperator is combined with the intercooler. The mass flow from the compressor exit is redirected to a heat exchanger located at the low-pressure turbine exit. There, the mass flow is heated up and fed into the combustion chamber (CC) inlet. Due to the preheated mass flow, less fuel needs to be burnt to reach the CC exit temperature T_{t4}. Using an intercooler, more heat can be recuperated, leading to higher efficiency [5].

AB-One's engines are optimized for cruise using GasTurb [76]. The objective of the optimization is a minimum thrust specific fuel consumption (TSFC) while providing a net thrust of $20\,kN$ respectively. The required thrust during cruise is derived from the glide ratio of 18.5. Additionally, the goal was to reach a reasonably small BPR to reduce nacelle drag and engine weight. However, a potential go-around limits the BPR minimization since AB-One needs to be able to perform this maneuver without help of ABB. Another aspect that needs to be considered for the choice of the BPR is the optimal use of the space between the vertical tail planes. Several engine layouts with different BPRs are calculated in GasTurb. If the BPR is too small, the engines are not able to provide enough thrust for go-around. Setting BPR to higher values improves TSFC on the one hand, but increases nacelle diameter. This prevents the engines placement in between the vertical tailplanes and increases parasitic drag. In this case, these aspects lead to a BPR of 8 for AB-One, which is used as an input parameter for the GasTurb optimization. With a resulting overall engine diameter of $1.9\,m$, the engines fit perfectly in between the V-Tail. Estimated polytropic engine component efficiencies are taken from [82] and are slightly improved according to [42], see table A.5. With a final TSFC of $13.003\,\frac{g}{kNs}$ the engines for AB-One are $22.4\,\%$ more efficient than an A320-200's IAE V2500 engine. This is also aided by the use of modern ceramic matrix composites turbine blades, that allow the high-pressure turbine inlet temperature to be $1573\,K$. These materials also allow high temperatures to be withstood without turbine blade cooling, increasing engine efficiency [29]. A relatively low overall pressure ratio of 23.89 allows the installation of special CC technologies that minimize NO_x production [78].

6 Levitation Landing

The landing gear of an A320-200 weighs approximately $2.5\,t$ [68]. While it is essential for safe taxiing, takeoff and landing, it is unnecessary weight that has to be carried throughout the flight. Research conducted by the GABRIEL [60] and GroLaS [50] projects investigate the possibility of landing and taking off with a ground based system. The research found the ground based system approach to be generally feasible. The systems described in this chapter are based on these projects and adapted for AB-One. The aircraft's landing gear is substituted by three force transmission points, see figure 6.2 and the wheels by a taxi cart, see figure 6.1.
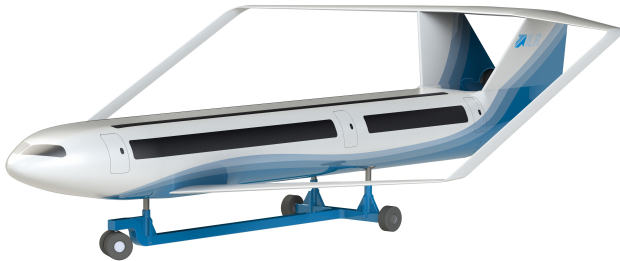
Figure 6.1: Taxi cart

The ground-system consists of two main components. The first one is the taxi cart holding the aircraft while on the ground, see figure 6.1. This cart is equipped with stilts that incorporate shock absorbers to dampen excess forces during landing and taxiing. It is also equipped with an electric motor and batteries to enable taxiing. The cart's batteries will also power AB-One's electrical systems during taxi so that the engines can remain switched off until takeoff. The second component is a magnetic levitation sledge. This maglev track holds a sledge on which these taxi carts, for various aircraft sizes and types, can be mounted. The mounting platform on the sledge can be rotated around the yaw-axis and move laterally to be positioned directly beneath the approaching aircraft. The sledge provides the aircraft with additional acceleration during takeoff and allows for quicker deceleration during landing, reducing takeoff and landing field lengths. This acceleration and deceleration are accomplished by a linear electric motor that is integrated into the track. Also, by incorporating magnetic levitation, rolling resistance can be substantially reduced.

Chapter 6. Levitation Landing
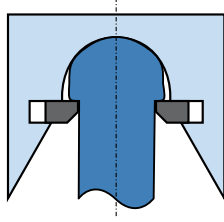
Figure 6.2: Force transmission point and locking mechanism

Since the sledge will be used to decelerate the aircraft at landing, it can be assumed that all energy this component needs for acceleration can be recuperated during landing. This is due to the fact, that the sledge only provides a portion of the takeoff thrust, but is the sole component decelerating the aircraft. Acceleration and deceleration is only limited by passenger comfort. The force transmission points inside AB-One's fuselage feature a locking-system, to prevent unintentional detachment from the cart. They are conically shaped, see figure 6.2, to make up for small deviations between the aircraft's and ground system's position during landing.

6.1 Takeoff Procedure

To avoid blocking the takeoff sledge because of engine failure, the engines are turned on and checked for functionality shortly before reaching the sledge. After successful engine check and confirmed disengagement of the cart's locking system, the taxi-cart rolls onto the sledge and is fixed in place automatically, see figure 6.3.

Figure 6.3: AixBox-One in preparation for takeoff

The aircraft is accelerated by the thrust of the main engines, the magnetic sledge and the booster. The main engines deliver a thrust of $142\,kN$ and are supported by another $84\,kN$ delivered by the magnetic sledge and another $172\,kN$ by the booster. This leads to a total thrust of $398\,kN$ and an acceleration of $0.5\,g$, which is within the range of bearable acceleration for the passengers [33]. To fully exploit the configuration's potential, the climb is split into three characteristic segments. For the first segment, the climb angle is set to 15 degrees for 2 minutes, while it is reduced to 10 degrees for another 3 minutes and 30 seconds for the second segment. ABB's detachment then occurs after 5 minutes and 45 seconds at flight level 250 (FL250), see figure 6.4. Besides shortening ABB's return distance, a high climb rate also reduces noise contours as the aircraft leaves the ground quicker. A higher climb rate demands higher thrust, which is provided by ABB. Reaching cruise flight level sooner allows the main engines to operate at their design point for a longer portion of the mission. The decision to detach ABB at FL250, and not at cruise flight level, keeps ABB's return distance reasonably short. The thrust for the last part of the climb is then provided by the main engines and the climb angle is reduced to 3 degrees. These two decisions lead to a required total takeoff thrust of 398 kN. Detailed information on thrust levels is broken down in chapter 9. With the MTOW of 79800 kg, the liftoff velocity equals $82.2\frac{m}{s}$, which is reached after a field length of 1700 meters.
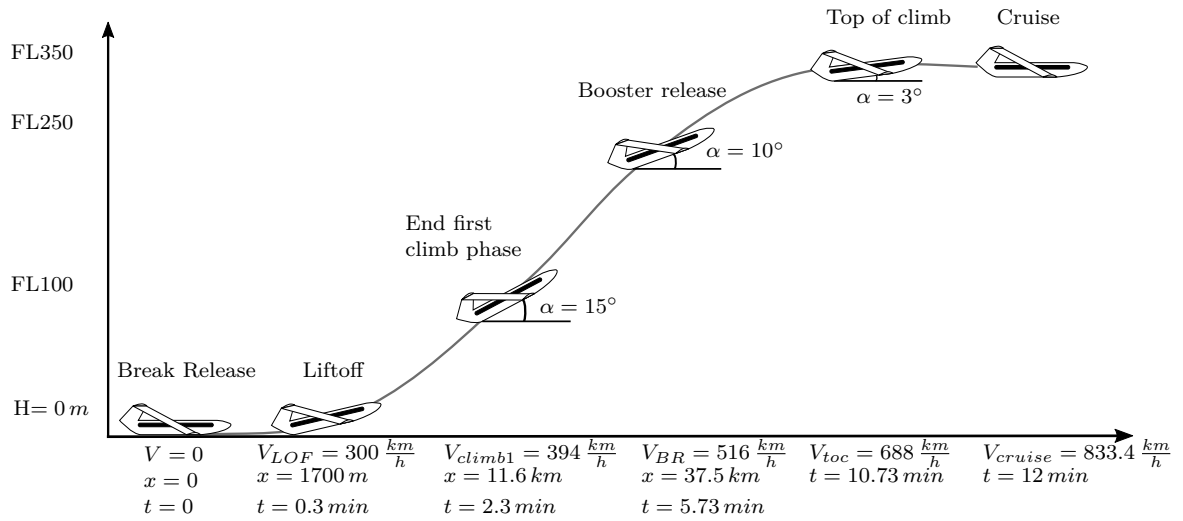
Figure 6.4: Takeoff and climb procedure

6.2 Landing Procedure

As usual, final approach is initiated at an altitude of approximately $1000\,ft$, 6 to $7\,km$ ahead of the runway threshold. The aircraft then flies with the so called target speed. When reaching the runway threshold, the velocity of the sledge and of the aircraft are synchronized. The sledge accelerates until the speed of the aircraft in glide position is met. With the help of the systems described above, sideslip, lateral displacement and pitch angle are compensated. AB-One lands like a conventional aircraft with a pitch angle. First the two backside force transmission points are locked at touchdown, after sufficient load is detected. After locking, breaking and with it, energy recuperation is initiated, reducing the aircraft's pitch angle, until the frontside force transmission point is locked. AB-One is then securely attached to the taxi cart. At the end of the runway, the taxi cart detaches from the sledge for taxiing.

6.3 Transition and emergency landing

Figure 6.5: Landing with sideslip and lateral displacement

During transition from conventional landing and takeoff to the ground based landing system, only few airports will be equipped with the required infrastructure. To guarantee a smooth transition phase, which is essential for the implementation of this system, two potential solutions are devised. To allow parallel operation of both landing systems, the maglev tracks are placed next to runways. Since not all airports are expected to be equipped with the system at the same time, an enhanced taxicart, capable of reaching takeoff speed is developed. At airports, that are still to be equipped with the maglev system, these carts are then used to fulfill the role of the magnetic sledge. Despite adding complexity and being far less efficient than the proposed sledge, they are deemed necessary to enable an economically viable transition. These carts are also used for emergency diversion airports. Those are airports that usually do not handle AB-One but are needed in order for safe flight routing. Since it would not be economical to install maglev systems at these

airports, the enhanced taxi cart is a good compromise to maintain operational freedom for route planning.
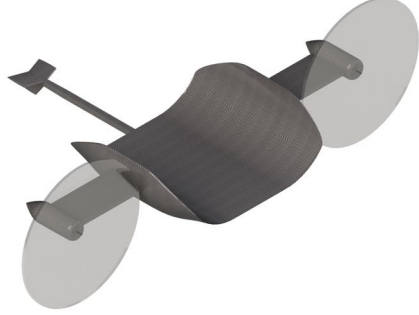
7 AixBox Booster

7.1 Introduction

Even though it represents the biggest portion of a civil airliners flight profile, modern airplane engines are usually not sized for cruise condition. This is caused by constraints that are derived from requirements such as takeoff field length and climb rates. In order to fill this gap between required thrust for takeoff as well as climb and thrust required for cruise, the AixBox Booster is developed. ABB is an electric support unit, that is attached to AB-One's fuselage for takeoff and climb providing additional thrust. At a certain flight level, ABB detaches from AB-One and then returns to the airport autonomously.

7.2 Design Process

To minimize design space for a novel system such as ABB, a number of decisions have to be made. First, the systems power source needs to be chosen. Compared to conventional aircraft propulsion systems, electric power trains have the advantage of being highly efficient, but come with a significant weight penalty as range increases [32, 72]. Since ABB is designed for a short mission range and to reduce gaseous and particle emissions around the airport, an electric power train is chosen. As the share of renewable energies is expected to increase [17], eventually, ABB will fly completely carbon neutral. ABB's weight is primarily dependent on battery and electrical system weight. The battery's volume is also a primary constraint in the design process of the ABB. Furthermore, ABB needs to be designed for three flight segments: delivering thrust for AB-One's takeoff, return flight and landing at the airport. In order to minimize drag during takeoff and climb the main body and battery compartment of ABB are designed to aerodynamically fit onto AB-One's fuselage. Two eight-blade propellers with variable blade pitch are chosen to ensure optimum efficiency across all operating speed regimes. Taking efficiency, ground clearance and inertia (for rapid control response) into account the propeller diameter is determined to be $5\,m$. To reduce energy consumption during return flight, the struts connecting ABB's main body to the engines are designed as airfoils to provide lift. For flight stability a vertical and a horizontal tailplane are added. These stabilizers are connected to ABB's main body by a strut and fit against AB-One's fuselage during climb to reduce interference drag. To land ABB, two alternatives are taken into consideration. The first being a horizontal landing on a runway and the second being a vertical hovering landing. First of all, landing horizontally would require a landing gear. Also, since ABB's landing speed would likely differ from regular aircraft, integration into airport operations would prove difficult. Finally, maximum slot capacity is already an issue at many airports, making landing horizontally less viable. Therefore, landing ABB vertically is considered to be the more practical option. To enable vertical landing the engine pods are mounted tiltable. This also proves useful for assembly of AB-One and ABB during turnaround. The two main propellers are counterrotating in order to allow for stable flight with the engines in a tilted position. To compensate for disturbances during hovering flight, a small propeller is mounted on the strut connecting the stabilizers and main body. This propeller is implemented as two-blade propeller to fit into a stowage compartment inside the strut, when it is not needed. Flight envelope tests have been conducted with a similar aircraft configuration to assess stability. According to that research ABB's three propeller configuration enables it to fly horizontally, vertically and to transition between both states [69]. The introduction of ABB also affects the design of AB-One. Since ABB delivers significant

amounts of thrust for AB-One during takeoff, AB-One's fuselage structure needs to accommodate a mounting mechanism able to transmit $170\,kN$. This incurs a weight penalty which has been accounted for in the fuselage weight estimation. ABB is positioned behind the front wing to be close to AB-One's center of gravity, but also to further accelerate the flow around the airfoil. This will provide extra lift while ABB is attached. AixBox Booster in both configurations can be seen in figure 7.1.

(a) ABB in takeoff configuration (as attached to AB-One)
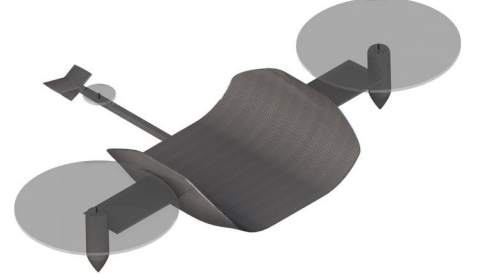
(b) ABB in landing configuration

Figure 7.1: AixBox Booster configuration

7.3 Power Train
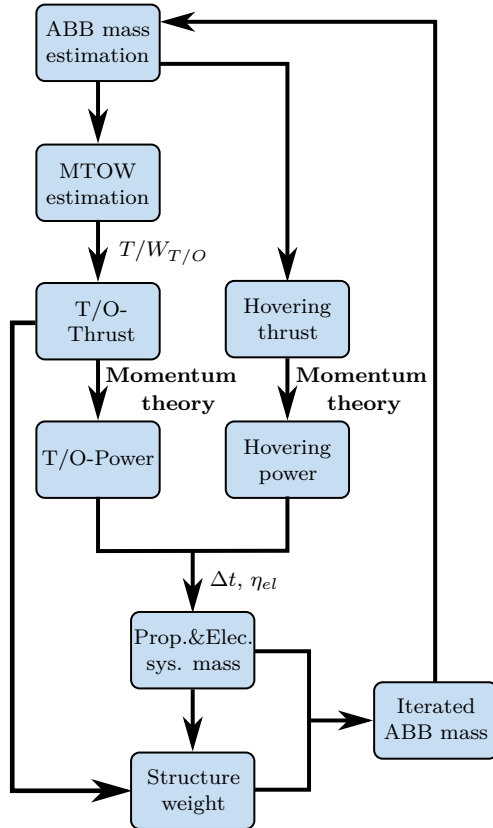
Figure 7.2: Iteration flow chart

ABB's thrust requirements are derived from the $(T/W)_{T/O}$ and the thrust provided by the engines during takeoff. Therefore, the thrust requirements depend on the MTOW of AB-One including ABB itself. Hence, a first estimation of ABB's weight is necessary. The calculation of ABB's final weight is then carried out iteratively. For that purpose an iteration scheme is developed, see figure 7.2. In order to allow for easy variation of the parameters and to keep the computational effort low, simple models such as momentum theory are used. As electric power supply Me-O_2 batteries are chosen. According to the Fraunhofer ISI prototypes of Me-O_2 batteries already reach gravimetric energy densities of $800\,\frac{Wh}{kg}$ whereas $1000\,\frac{Wh}{kg}$ is the predicted maximum. Market entry is expected for 2030 [72], hence further refinement of the technology is expected until 2045. Yet, since the full potential is not expected to be exhausted until 2045 a value of $900\,\frac{Wh}{kg}$ is chosen as gravimetric energy density. The battery's capacity is sized according to the flight mission described in chapter 9. With the more detailed technical data on the propellers, motors, inverters and batteries given in table 7.1, the weight of the electrical systems can be estimated to be around $2400\,kg$ providing $4.1\,MW$ of shaft power per engine. For a rough estimation of structure weight, ABB was assumed as a straight beam with a constant closed hollow rectangular cross section. Considering the required thrust and the implied loads during takeoff and landing the structure weight is estimate to be

around $1240\,kg$. The weight of the propellers is scaled to the same power loading per propeller mass

as the A400M's FH385/FH386 [18], yielding a weight of $380\,kg$ per propeller. These component masses add up to a total weight of around $4400\,kg$.

Table 7.1: Technical data of the power train [77]

Propeller	Efficiency: 90 %	Diameter: $5\,m$
Motor	Efficiency: 96 %	Specific power: $13\,\frac{kW}{kg}$
Inverter	Efficiency: 98 %	Specific power: $16.5\,\frac{kW}{kg}$
Battery	Vol. energy density $570\,\frac{Wh}{l}$	Grav. energy density: $900\,\frac{Wh}{kg}$

7.4 Flight Operations

During climb the booster is attached to AB-One providing thrust at maximum shaft power. Reaching FL250, ABB detaches from AB-One and enters return flight. Compared to the reference aircraft, this climb segment is significantly shorter. Due to its airfoils, ABB can gradually tilt its rotors into an upright position while maintaining a controlled descent. Furthermore, the power output of ABB's engines can be reduced drastically, since 25% of maximum power are sufficient to keep ABB in stationary hovering flight. Utilizing the airfoils, actual power consumption can be expected to be significantly lower. A potential flight trajectory for return flight is shown in figure 7.3 by the example of Madrid-Barajas (LEMD) [14]. The trajectory does not cross any other trajectories on the same flight level. ABB approaches the airport perpendicular to the active runway in order avoid other airtraffic. Reaching the airport ABB lands vertically on the booster ground support vehicle (BGSV), see figure 7.4(a).
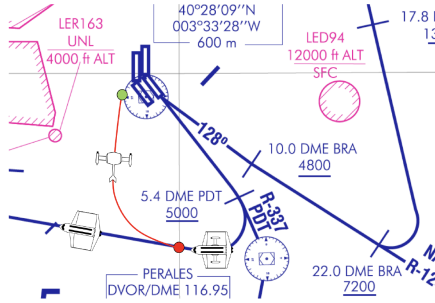
Figure 7.3: Proposed trajectory for ABB [14]

Since ABB has to operate above densely populated areas, reliable emergency strategies are mandatory. In case of engine failure ABB enters autorotation. By use of the above-mentioned tailplanes and collective blade pitch adjustment on both main rotors, maneuverability can be retained to a certain degree. Finding a safe landing site is essential in order to avoid endangering people or critical infrastructure. Several research projects investigated the evaluation of possible landing sites via machine learning and yield satisfying results [28, 51, 3, 48]. Control strategies for unmanned aireal vehicles in autorotation to reach a determined landing site including obstacle avoidance have also been developed in recent research [11, 71, 81]. Considering the fast development of machine learning algorithms, emergency procedures of ABB are not expected to be an issue during certification.

7.5 Ground Operations

In order to keep ground operations as simple as possible, the automated booster ground support vehicle is designed. BGSV is an electric cart equipped with a lifting mechanism, and an interface structure for ABB to land on, see figure 7.4(a).

After Landing on BGSV, ABB is carried to a battery swapping station. With a new battery installed, BGSV carries ABB to the next aircraft that is being prepared for takeoff. BGSV then lifts the

(a) ABB landing on BGSV

(b) ABB being mounted to AixBox One
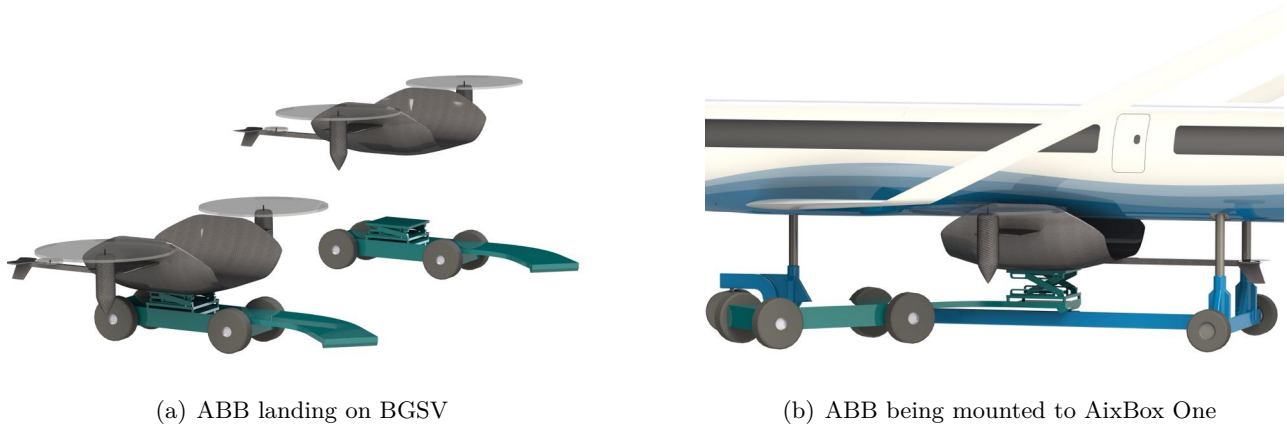
Figure 7.4: ABB ground operations

Booster unit up against the aircraft's fuselage, where it latches on to the mounting mechanism, see figure 7.4(b). The taxi cart's height is chosen appropriately to leave enough room for BGSV and ABB to fit underneath the fuselage for assembly. To estimate the number of boosters needed to ensure smooth flight operations, departure records provided by Fraport AG are evaluated [22]. For different representative days, the numbers of aircraft belonging to the A320 and B737 families are counted and interpreted. These aircraft are chosen because they cover the market segment that AB-One is aiming for. On average, Frankfurt Airport (EDDF), which is one of the largest hubs in Europe, handles 30 aircraft of this size per hour, peaking at 45 aircraft per hour. ABB's mission was estimated to be 40 minutes, which includes 10 minutes for takeoff, 10 minutes for return and 20 minutes for battery swapping, taxiing and reattachment. This leads to a minimum number of 30 ABBs to ensure smooth flight operations. Five additional ABBs should be held available to cover maintenance duration, leading to a total number of 35 ABBs for Frankfurt airport. Instead of recharging ABB directly, battery swapping is chosen. This is done to achieve significantly shorter turnaround times, but also to prolong battery life. This is achieved by applying optimized charging methods that require more time to avoid overheating associated with high charging currents [34].These methods can be used, because with battery swapping, charging time is no longer a constraint. In order to recharge enough batteries to maintain an average of 30 departures per hour, $34.8\,MW$ of electricity is needed. Even though this is an unusual high demand, there are already facilities using similar amounts of power[20], so providing enough electricity is not considered an issue. Having such a large amount of batteries in one system also opens up the possibility to use these to stabilize the energy grid. Especially with growing numbers of intermittent renewable energy sources that require storage capacities, this opportunity should be considered [21, 17, 54].

8 Mass and Center of Gravity

The mass is estimated according to empirical formulas in [56, 61, 73]. To estimate the boxwing's weight, a formula that is specifically dedicated for the purpose of boxwings, is applied [53]. Based on the wing characteristics, it considers the mass of each wing, the connected wingtip and the reduced wing box weight resulting from a lower structural load. The results can be found in table 8.1. The fuel is notably reduced compared to the A320-200. As it is shown in chapter 9, the energy consumption of AB-One is minimized to approximately $33\,\%$ of the A320-200, with respect to the different range and passenger number. Therefore, AB-One only needs to carry a small mass of fuel for the design mission.

Chapter 8. Mass and Center of Gravity

Figure 8.1 shows the Payload-Range diagram of AB-One with the high payload, but a reduced range as stated in chapter 1.

Table 8.1: Component mass

Component	AixBox One in [kg]	A320-200 in [kg]
Fuselage	12840	8900
Wing	8775	8100
VTP	1033	680
HTP	0	520
Landing gear	0	2500
Pylon	0	1240
Propulsion	4100	7750
Booster	4400	0
Systems	5306	5400
Furnishings	4393	3000
Operational items	3692	3900
Fuel	9079	18635
OEW	44534	41990
MEW	40843	38090
Strucure Weight	22748	21940
MZFM	70721	58990
MTOW	79800	77625

Table 8.2: Center of gravity

CG Case	With ABB in [m]	Without ABB in [m]
Design Case	21.95	22.29
$x_{CG,noPayload,noFuel}$	22.66	23.39
$x_{CG,maxPayload,noFuel}$	21.84	22.20
$x_{CG,maxPayload,maxFuel}$	21.87	22.20
$x_{CG,PayloadToMTOW,maxFuel}$	21.95	22.41
$x_{CG,noPayload,maxFuel}$	22.60	23.19
$x_{CG,front}$	21.84	22.20
$x_{CG,aft}$	22.66	23.39

The related CG for all flight cases is listed in table 8.2. The cases with booster and without booster are portrayed as well as the foremost and aftmost CG. To keep the balance in the moment of detaching the booster, the booster is positioned as close as possible to the CG of the aircraft. Due to a changing CG, this cannot be done completely accurate. Therefore, any resulting moments are balanced out by shifting fuel to the front of the aircraft [26].
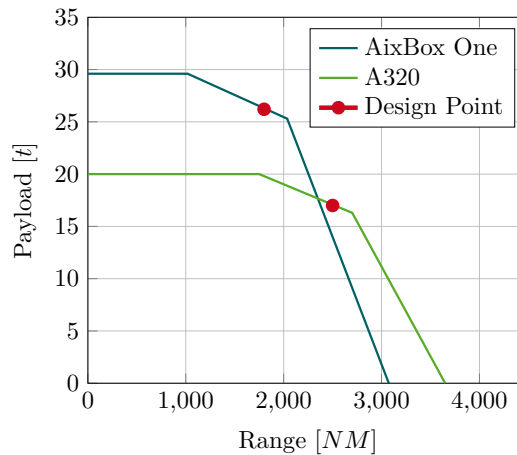

Figure 8.1: Payload - Range diagram

Comparing the CG with the allowable range of CG ($21.5\,m$ to $22.71\,m$) from the longitudinal stability analysis in chapter 4.1, some exceptions have to be made. The red colored values are out of range. However, the case of "maximum fuel and no booster" is not decisive since the booster is be released

after the climb segment, where some fuel is already burned. If, in this case, the fuel from the aft tank is used, the CG will not leave the allowed range. Moreover, the case of "no payload and no fuel" is also not a limiting factor. If the flight mission is very short, it can be considered to leave the booster attached to the aircraft until landing. If not, at least $2\,t$ of fuel need to be kept in the front wing for stability. With these assumptions, the aircraft is evaluated as stable within the scope of this predesign.

9 Energy Calculation

An energy consumption calculation is performed to evaluate AB-One's performance against the A320-200 baseline aircraft. The mission profile for the A320-200 was generated using the MICADO software [36]. To determine the total energy required to fly the reference mission, the block fuel calculated by MICADO, was multiplied with the heat value of Jet-A kerosene. This leads to a total energy consumption of 158.835 MWh for a 1800 NM mission with 150 passengers. To obtain a decent estimation for AB-One's energy consumption, the design mission is split into several representative segments, see table 9.1.

Table 9.1: Energy consumption

	Takeoff	Climb FL100	Climb FL250	Climb FL350	Cruise	Descent, Landing	ABB return, and safety
Total thrust req. [kN]	398.27	226.38	160.57	64.24	40	5	-
TF thrust req. [kN]	142.33	155.9	105.2	64.24	40	5	-
ABB thrust req. [kN]	171.94	70.48	55.37	-	-	-	-
Catcher thrust [kN]	84	-	-	-	-	-84	-
ABB shaft power output per Eng.[MW]	4.1	4.1	4.1	-	-	-	-
ABB power input [MW]	9.69	9.69	9.69	-	-	-	-
Main engine power input [MW]	38.64	63.59	47.56	34.26	22.63	2.58	-
Total power input [MW]	43.41	73.28	57. 25	34.26	22.63	2.58	-
Time [min]	0.3	1.99	3.43	5	217.05	23.48	-
Total energy [MWh]	0.22	2.44	3.27	2.85	81.85	1.01	0.383
Angle of climb [°]	0	15	10	3	0	-3.3	-
Distance covered [NM]	0	6.13	13.98	25.44	1654.43	100	20.12

The first segment is takeoff, where ABB is attached to AB-One and providing thrust. Also, additional thrust is provided by the ground based takeoff and landing system. However this thrust is not taken into account for the total energy consumption calculation, since it is assumed that this energy will be recuperated during landing, see chapter 6. The climb-phase where ABB is attached, is split into two segments to account for changing atmospheric conditions and a higher Mach number. The angle of climb is chosen as high as economically possible, to shorten ABB's airport return distance and reduce the noise contours. ABB's thrust for different atmospheric densities and airspeeds is calculated using actuator disk theory. ABB is expected to run at full shaft power for the entire climb, since the electrical power train has a higher efficiency than the turbofan engines. TSFC for these segments is calculated using GasTurb. ABB separates from AB-One at FL250. This leads to a short return distance for ABB while considering the turbofan-engines' performance restrictions. FL350 is reached after approximately 11 minutes. During this segment the propulsion-concept shows its largest benefit due to the cruise optimized main engines. For descent and landing an average thrust level and TSFC are assumed. The energy consumed by ABB for return to the airport is taken from ABB's power

train sizing iteration loop. Due to ABB's high T/W, the propellers only need to operate at roughly 25 % percent power to enable hovering. For this calculation the whole return flight was calculated as hovering, which is a very conservative estimation. To allow for safer operations, additional energy for operating 2 minutes at full throttle is included in this calculation. On its design mission of $1800\,NM$, carrying 264 passengers, AB-One consumes $92.024\,MWh$, including ABB and it's return. This leads to the following energy consumption per passenger, and provides savings up to 67 %, see table 9.2.

Table 9.2: Energy per passenger in MWh

2 Class per PAX Energy AB-One	0.3486
2 Class per PAX Energy A320	1.0589
Energy Savings 2 Class [%]	67.08
1 Class per PAX Energy AB-One	0.2823
1 Class per PAX Energy A320	0.8539
Energy Savings [%]	66.94

10 Noise

Noise reduction is an important objective during airplane design. However, this work is focused on energy efficiency, therefore reducing energy consumption is the main design driver. While engine noise dominates the aircraft's noise profile during takeoff, landing gear and high lift devices are the dominating components in landing configuration [46]. AB-One's main engines are placed on top of the fuselage between vertical tailplanes. Hence, the engine noise is shielded effectively during takeoff. Furthermore, the turbofan engines feature chevrons to reduce noise behind the engine. Compared to the reference aircraft, AB-One performs an overall steeper and faster climb reducing the noise contours significantly. Since AB-One comes without a landing gear, noise production during landing is also decreased substantially. Considering the design of the taxi cart as a first draft, it can be optimized further regarding noise reduction. Still, the propeller noise of ABB has to be considered. To predict the propeller noise, the estimation method according to Hamilton Standard was used [80]. All sound pressure levels are given at a distance of $500\,ft$ in the propeller plane. Assuming an eight-blade propeller with a tip Mach number of 0.8 predicts a sound pressure level per propeller of $99\,dB$ during takeoff and $89\,dB$ during landing. While sound pressure levels values in general lack comparability, this value does not seem unreasonable. Nonetheless, the effect of the front wing's wake onto the propellers' noise production is difficult to quantify without immense computational effort and therefore is neglected. However, the overall noise level of the propeller is expected to increase due to the disturbed inflow. Based on these estimations, the system's overall noise level is predicted to remain roughly the same during takeoff, but to decrease substantially during landing.

11 Technology List

The following list shows the prospective technologies and why they are available in the near future.

- **Transparent structure for panorama window**: The Institute of Textile Technology at RWTH Aachen University is already doing research in transparent materials. The materials are expected to be more than 90 % transparent, pressure resistant and therefore, be applicable for an aircraft [6].

- **Energy density of** $900\,Wh/kg$ **for booster batteries** : According to the Fraunhofer ISI prototypes already reach gravimetric energy densities of $800\,Wh/kg$. Market entry is expected for 2030, hence further refinement of the technology is expected until 2045 [72].

- **Emergency landing site detection via machine learning**: Several studies have been performed proving the algorithms to work properly. Considering the fast developments in the field of machine learning the technology is expected be ready for use outside of academics [3, 28, 48, 51].

- **Ground based landing system**: mb+Partner already performed a profound feasibility analysis including risks, costs, and operability. They state a ground based landing system as generally feasible. IATA expects the technology to be available 2032 [39].

- **Electrical driven cart for aircraft ground operations**: Electric cars are already established and range is not a limiting factor for airport operations. Autonomous cars are already able to cover significant distances withouth disengaging. Therefore, in the controlled environment of an airport autonomous driving is not considered an issue [2].

- **Riblet surface**: Nowadays CFD-Simulations indicate that an optimized surface for less wall shear stresses is possible and therefore, a suitable riblet surface for an aircraft is evaluated as realistic until 2045.

- **Improved core efficiencies**: Polytropic engine component efficiencies are taken from [82] and slightly improved according to the development prospected by [42].

- **BLI with minimized inlet distortion**: Boundary layer ingestion offers significant fuel savings [74], inlet distortion effects can be mitigated through none axisymmetric stator geometry [30].

- **Advanced materials**: Extrapolating from observed advances, weight savings of 10 % due to use of advanced composite materials are expected.

12 Conclusion and Outlook

The AixBox One introduces an innovative aircraft concept featuring a boxwing configuration and a hybrid modular propulsion system to meet and exceed the ambitious goals set by DLR and NASA. While flying purely electric proves to be difficult due to the required gravimetric energy density, the AixBox Booster allows AixBox One to benefit significantly from the superior efficiency of electric propulsion systems. The AixBox Booster allows AB-One's engines to be downsized and optimized for cruise, reducing specific fuel consumption by 22.3 %. Furthermore, the design point for cruise flight can be set to high wing loadings resulting in a relatively small wing area and low weight. To deal with the forecasted market development, AB-One is designed with a double bubble fuselage increasing overall passenger capacity by 76 % while only increasing the total wetted surface by 21.1 %. The introduction of the ground based landing system spares the need for a landing gear resulting in a significant reduction of weight. Moreover, the absence of a landing gear reduces C_{D0} and noise levels during takeoff and landing. Due to the boxwing configuration the induced drag coefficient is reduced by 10.8 % compared to the A320-200. In combination with the double bubble fuselage, AixBox One's dimensions can remain in the same order of magnitude as the A320-200's, while reducing C_{D0} by 13.2 %. Energy consumption is reduced by 67 % per passenger. A large proportion of these improvements can be attributed to the introduction of ABB, the ground based landing system, the boxwing configuration, and the double bubble fuselage. However, the impact of further optimization of proven technologies should not be neglected. For a list of expected technological advances incorporated in this concept study, refer to chapter 11.

Since this is a preliminary design study, calculations are mostly kept to empirical formulas, while further analytical investigations are performed for design critical matters. In order to advance this concept, high fidelity analysis would have to be performed. The introduction of an electric propulsion system requires further investigation into battery technologies, power electronics and the thermal

management of these systems. For aerodynamics, sophisticated computational fluid dynamic studies and wind tunnel tests would have to be performed. Special attention should be paid to stability problems of AB-One and the overall aerodynamic design of ABB. Regarding structural design, detailed analysis of the structures aeroelastic behaviour is recommended. The force transmission from ABB to AB-One, as well as the structural design of a boxwing's fuselage and wing should also be looked at. Further attention should be paid to the boxwing configuration in regard to total direct operating costs associated with it's span, taking ICAO boxes and drag into account.

This work features a variety of new systems. While these are expected to offer significant savings, their introduction is also associated with major financial investments. It is noted that implementing all systems simultaneously is a very ambitious goal due to the high upfront costs. However, since ABB, AB-One's configuration, and the ground based landing system already offer significant energy reduction as standalone systems, a successive introduction is possible.

It should also be noted, that novel concepts require special attention to certification. Yet, certification of AB-One is not expected to present major complications. Conventional certification requirements such as evacuation and emergency situations, for example one engine out, are taken into account. Novel systems such as ABB and the ground based landing system are assessed for possible risks, and solutions are presented. Finally, there are several additional possibilities to further improve this concept. However, incorporating all these is beyond the scope of this work. To name a few, advanced biofuels can be used to reduce the carbon footprint and NOx emissions. Morphing structures are also an intriguing concept, but so far lack reliable design approaches.
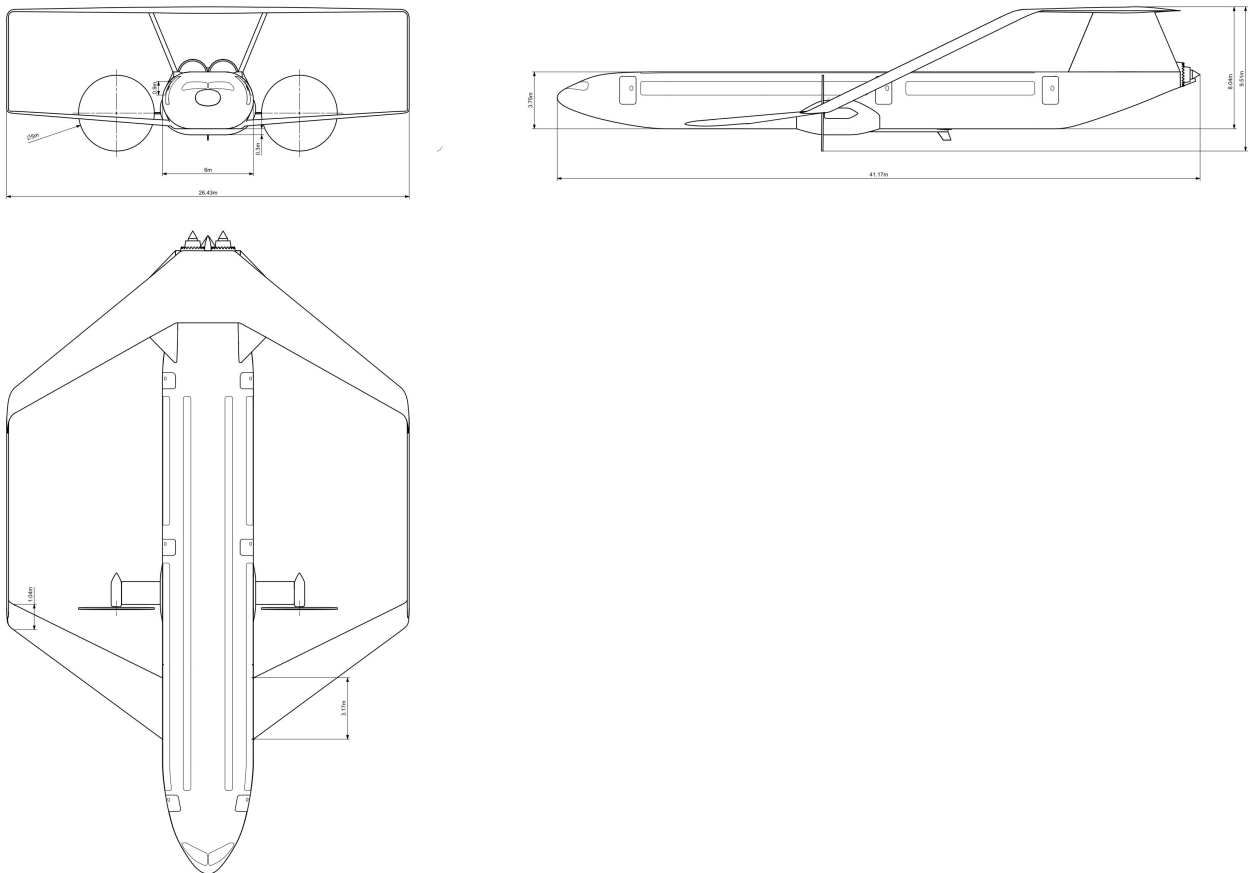

Figure 12.1: Multiview orthographic projection

Bibliography

[1] AIRBUS: *Global Market Forecast 2017-2036: Growing Horizons.* URL https://www.airbus.com/content/dam/corporate-topics/publications/backgrounders/Airbus_Global_Market_Forecast_2017-2036_Growing_Horizons_full_book.pdf, 2017. – ISBN 978-2-9554382-2-6

[2] AOKI, R.: *Report on Autonomous Mode Disengagements: For Waymo Self-Driving Vehicles in California.* Department of Motor Vehicles, Licensing and Operation Division, 2017. – URL https://www.dmv.ca.gov/portal/wcm/connect/42aff875-7ab1-4115-a72a-97f6f24b23cc/Waymofull.pdf?MOD=AJPERES

[3] AZIZ, S. ; FAHEEM, R. M. ; BASHIR, M. ; KHALID, A. ; YASIN, A.: Unmanned Aerial Vehicle Emergency Landing Site Identification System Using Machine Vision. In: *Journal of Image and Graphics* 4 (2016), Nr. 1. – URL http://www.joig.org/uploadfile/2016/0603/20160603080042521.pdf

[4] BERSTER, P. ; DOYRAN, D. ; GELHAUSEN, M. ; GRIMME, W. ; HEPTING, M. ; LEIPOLD, A. ; MAERTENS, S. ; PABST, H. ; WILKEN, D. ; DEUTSCHES ZENTRUM FÜR LUFT- UND RAUMFAHRT E.V. (Hrsg.): *Luftverkehrsbericht 2016: Daten und Kommentierungen des deutschen und weltweiten Luftverkehrs.* 2017. – URL http://www.dlr.de/fw

[5] BOGGIA, S. ; RÜD, K.: Intercooled Recuperated Gas Turbine Engine Concept. In: AMERICAN INSTITUTE OF AERONAUTICS AND ASTRONAUTICS (Hrsg.): *41st AIAA/ASME/SAE/ASEE Joint Propulsion Conference & Exhibit.* Tuscon, Viriginia : American Institute of Aeronautics and Astronautics, 07102005. – ISBN 978-1-62410-063-5

[6] BRÜLL, R. ; SEIDE, G. ; GRIES, T.: *Advances in The Production of Transparent Fiber Reinforced Thermoplastics.* Aachen, Deutschland : Institut für Textiltechnik, RWTH Aachen University, 2017

[7] BÜTTNER, C. C.: *Shark Skin Inspired Surfaces For Aerodynamically Optimized High Temperature Applications - Fabrication, Oxidation, Characterization*, RWTH Aachen University, Dissertation, 2011. – URL http://publications.rwth-aachen.de/record/64468/files/3689.pdf

[8] CAJA, R. ; SCHOLZ, D.: *Box Wing Flight Dynamics in the Stage of Conceptual Aircraft Design.* Hamburg, Deutschland : Aero – Aircraft Design and Systems Group, Hamburg University of Applied Sciences, 2012. – URL http://www.dglr.de/publikationen/2012/281383.pdf

[9] CHEMIE.DE ; LUMITOS GMBH (Hrsg.): *Bredtsche Formel.* 1997. – URL http://www.chemie.de/lexikon/Bredtsche_Formel.html

[10] CILIBERTI, D. ; NICOLOSI, F. ; VECCHIA, P. D.: *A new Approach in Aircraft Vertical Tailplane.* Neapel, Italien : Deptartment of Industrial Engineering, University of Naples "Federico II", 2013 (XXII Conference)

[11] DALAMAGKIDIS, K.: *Autonomous vertical autorotation for unmanned helicopters.* Florida, University of South Florida, Dissertation, 2009. – URL https://pdfs.semanticscholar.org/6e12/c0f3c658181b1b8cefc22c48c3c7a975ed5f.pdf

[12] DLR-KOMMUNIKATION: Das Deutsche Zentrum für Luft- und Raumfahrt: Broschüre. (2011). – URL https://www.dlr.de/Portaldata/1/Resources/ueber_dlr/DLR_Broschuere.pdf

Bibliography

[13] DRELA, M.: *D8.x Aircraft Development: Update.* Aero & Astro Presentation, 2010. – URL http://web.mit.edu/drela/Public/N+3/tasaa.pdf

[14] ENAIRE: *Carta de Salida Normalizada: Vuelo por Instrumentos.* Servicio de información aeronáutica (AIS-Espana), 2018. – URL https://ais.enaire.es/AIP/AIPS/AMDT_303_2018_AIRAC_06_2018/AIP.html

[15] ENGINEERING TOOLBOX: *Barlow's Formula - Internal, Allowable and Bursting Pressure: Calculate pipes internal, allowable and bursting pressure.* 2005. – URL https://www.engineeringtoolbox.com/barlow-d_1003.html

[16] EUROPÄISCHE KOMMISSION: *Flightpath 2050: Europe's vision for aviation ; maintaining global leadership and serving society's needs - report of the High-Level Group on Aviation Research.* 2011. – URL https://ec.europa.eu/transport/sites/transport/files/modes/air/doc/flightpath2050.pdf

[17] EUROPÄISCHE KOMMISSION: *GRÜNBUCH: Ein Rahmen für die Klima- und Energiepolitik bis 2030.* 2013. – URL https://eur-lex.europa.eu/legal-content/DE/ALL/?uri=CELEX:52013DC0169

[18] EUROPEAN AVIATION SAFETY AGENCY: *Type-Certificate Data Sheet: for Propeller FH385/FH386 series.* European Aviation Safety Agency, 2015. – URL https://www.easa.europa.eu/sites/default/files/dfu/TCDS%20P%20012%20-%20FH385-FH386%20Series%20-%20Issue04%20_20151512_1.0.pdf

[19] EUROPEAN AVIATION SAFETY AGENCY: Certification Specifications and Acceptable Means of Compliance for Large Aeroplanes CS-25. (2018), Nr. 21. – URL https://www.easa.europa.eu/sites/default/files/dfu/CS-25%20Amendment%2021%20v1.pdf

[20] EUROPEAN TRANSONIC WINDTUNNEL GMBH: *Aerodynamic Circuit.* Köln, Deutschland, 2004. – URL https://www.etw.de/wind-tunnel/aerodynamic-circuit

[21] EVANS, A. ; STREZOV, V. ; EVANS, T. J.: Assessment of utility energy storage options for increased renewable energy penetration. In: *Renewable and Sustainable Energy Reviews* 16 (2012), Nr. 6. – ISSN 13640321

[22] FRANKFURT AIRPORT SERVICES WORLDWIDE ; FRAPORT AG (Hrsg.): *Flüge - alle Informationen zu Ihrem Flug: Abflüge.* 2018. – URL https://www.frankfurt-airport.com/de/reisen/am-flughafen.overview.fluege.html

[23] FREDIANI, A. ; GASPERINI, M. ; SAPORITO, G. ; RIMONDI, A.: *Development of a Prandtlplane Aircraft Configuration.* Pisa, Italien : Department of Aerospace Engineering "Lucio Lazzarino", Pisa University, 2003. – URL https://pdfs.semanticscholar.org/6ec0/b11d9d309171fed9d174860a3fb30e3fbaa9.pdf

[24] FUCHTE, J. C.: *Enhancement of Aircraft Cabin Design Guidelines with Special Consideration of Aircraft Turnaround and Short Range Operations.* Hamburg, Deutschland, Technischen Universität Hamburg-Harburg, Dissertation, 2014. – URL https://elib.dlr.de/89599/1/Fuchte%20FB-2014-17%20Version%20Druck.pdf

[25] GAMRATH, D. N.: *Boeing Global Airport Congestion Study: Market Analysis 2015 Study Update.* Boeing, 2014. – URL https://www.aci-na.org/sites/default/files/07_-_global_airport_congestion.pdf

Bibliography

[26] GATTING, M.: *Untersuchung der Flugeigenschaften von Flugzeugen anhand der Phygoidbewegung.* Bremen, Deutschland : Hochschule Bremen (FH)

[27] GLOUDEMANS, J. R. ; AND OTHERS FOR NASA SINCE THE EARLY 1990's: *OpenVSP.* 2012. – URL `openvsp.org`

[28] GUO, X. ; DENMAN, S. ; FOOKES, C. ; MEJIAS, L. ; SRIDHARAN, S.: Automatic UAV Forced Landing Site Detection using Machine Learning. In: BOUZERDOUM, Abdesselam (Hrsg.): *2014 International Conference on Digital Image Computing: Techniques and Applications (DICTA).* Piscataway, NJ : IEEE, 2014. – ISBN 9781479954094

[29] HALBIG, M. C. ; JASKOWIAK, M. H. ; KISER, J. D. ; ZHU, D.: *Evaluation of Ceramic Matrix Composite Technology for Aircraft Turbine Engine Applications.* American Institute of Aeronautics and Astronautics, Inc, 2013. – URL `https://ntrs.nasa.gov/archive/nasa/casi.ntrs.nasa.gov/20130010774.pdf`

[30] HALL, D. K. ; GREITZER, E. M. ; TAN, C. S.: Analysis of Fan Stage Conceptual Design Attributes for Boundary Layer Ingestion. In: *Journal of Turbomachinery* 139 (2017), Nr. 7, S. 1–12

[31] HEATHROW AIRPORT: *Airports Commission: Long-term hub capacity options: Heathrow Airport Limited response.* 2013. – URL `https://www.heathrow.com/file_source/Company/Static/PDF/Companynewsandinformation/long-term-hub-capacity-options_LHR.pdf`

[32] HEPPERLE, M.: *Electric Flight: Potential and Limitations.* Braunschweig, Deutschland : Deutsches Zentrum für Luft- und Raumfahrt e.V., 2012. – URL `https://www.mh-aerotools.de/company/paper_14/MP-AVT-209-09.pdf`

[33] HOBEROCK, L. L.: *A Survey of Longitudinal Acceleration Comfort Studies in Ground Transportation Vehicles: Research Report 40.* Austin, Texas : Council for Advanced Transportation Studies, University of Texas at Austin, 1976

[34] HOKE, A. ; BRISSETTE, A. ; SMITH, K. ; PRATT, A. ; MAKSIMOVIC, D.: Accounting for Lithium-Ion Battery Degradation in Electric Vehicle Charging Optimization. In: *IEEE Journal of Emerging and Selected Topics in Power Electronics* 2 (2014), Nr. 3, S. 691–700

[35] HÖRNSCHEMEYER, R.: *Übung 10 Flugzeugbau II - Stabilität & Steuerbarkeit.* Aachen, Deutschland : Institut für Luft- und Raumfahrtsysteme, RWTH Aachen University, 2017

[36] INSTITUT FÜR LUFT- UND RAUMFAHRTSYSTEME, RWTH AACHEN UNIVERSITY: *Multidisciplinary Integrated Conceptual Aircraft Design and Optimization Environment (MICADO).* 2010. – URL `http://www.ilr.rwth-aachen.de/index.php?id=359`

[37] INSTITUT FÜR STATIK UND DYNAMIK, GOTTFRIED WILHELM LEIBNIZ UNIVERSITÄT HANNOVER: *STAB2D.* 2005. – URL `https://www.isd.uni-hannover.de/stab2d.html`

[38] INTERNATIONAL AIR TRANSPORT ASSOCIATION: Fact Sheet Climate Change & CORSIA. (2018). – URL `https://www.iata.org/pressroom/facts_figures/fact_sheets/Documents/fact-sheet-climate-change.pdf`

[39] INTERNATIONAL AIR TRANSPORT ASSOCIATION ; DEUTSCHES ZENTRUM FÜR LUFT- UND RAUMFAHRT E.V. ; GEORGIA INSTITUTE OF TECHNOLOGY ; INTERNATIONAL AIR TRANSPORT ASSOCIATION (Hrsg.): *Technology Roadmap.* 2013. – URL `https://www.iata.org/whatwedo/environment/Documents/technology-roadmap-2013.pdf`

Bibliography

[40] International Civil Aviation Organization: Aerodrome Design Manual: Part 1 Runways: Approved by the Secretary General and published under his authority. (2006), Nr. 3

[41] Jenkinson, L. ; Simpkin, P. ; Rhodes, D.: *Civil Jet Aircraft Design.* Washington, DC : American Institute of Aeronautics and Astronautics, Inc, 1999. – ISBN 978-1-56347-350-0

[42] Konstantinos, G.: Future Aero Engine Designs: An Evolving Vision. In: Benini, E. (Hrsg.): *Advances in Gas Turbine Technology.* InTech, 2011. – ISBN 978-953-307-611-9

[43] Kroo, I.: Nonplanar Wing Concepts For Increased Aircraft Efficiency. In: *Innovative Configurations and Advanced Concepts for Future Civil Aircraft* (2005). – URL http://aero.stanford.edu/reports/vki_nonplanar_kroo.pdf

[44] Lammering, T. ; Schneider, T. ; Stumpf, E.: The Right Single-Aisle for the Future Market. In: American Institute of Aeronautics and Astronautics (Hrsg.): *53rd AIAA Aerospace Sciences Meeting.* Reston, Virginia, 2015, S. 40. – ISBN 978-1-62410-343-8

[45] Lange, R. H. ; Cahill, J. F. ; Bradley, E. S. ; et al.: *Feasibility Study of the Transonic Biplane Concept for Transport Aircraft Application: Research report prepared under contract NAS1-12413 on behalf of the National Aeronautics and Space Administration.* Marietta, Georgia : The Lockheed-Georgia Company, 1974. – URL http://ntrs.nasa.gov/archive/nasa/casi.ntrs.nasa.gov/19740026364_1974026364.pdf

[46] Langley Research Center ; NASA Administration (Hrsg.): *NASA's Quiet Aircraft Technology Program: Reducing Aircraft Noise to Improve Our Quality of Life.* – URL https://www.nasa.gov/centers/langley/pdf/70882main_FS-2002-09-73-LaRC.pdf

[47] Leahy, J.: *Global Market Forecast 2013-2032.* Airbus, 2013. – URL http://www.airbus.com/newsroom/news/en/2013/09/global-market-forecast-2013-2032-continuing-the-trend-toward-larger-and-more-efficient-a.html

[48] Li, X.: A Software Scheme for UAV's Safe Landing Area Discovery: 2013 AASRI Conference on Intelligent Systems and Control. In: *AASRI Procedia* 4 (2013). – ISSN 22126716

[49] Liebeck, R. H.: Design of the Blended Wing Body Subsonic Transport. In: *Journal of Aircraft* 41 (2004), Nr. 1. – ISSN 0021-8669

[50] mb + Partner ; Ingenieure Marquardt & Binnebesel, Partnerschaft, Luftfahrt-Technologie (Hrsg.): *GroLaS-Technologie.* 2010. – URL www.mbptech.de

[51] Mukadam, K. ; Misarwala, F. ; Sinh, A. ; Karani, R.: Detection of Landing Areas for Unmanned Aerial Vehicles. In: *International Journal of Computer Applications (IJCA)* 131 (2015), Nr. 2

[52] NASA Aeronautics: Strategic Implementation Plan 2017 Update. (2017), Nr. NP-2017-01-2352-HQ. – URL https://www.nasa.gov/sites/default/files/atoms/files/sip-2017-03-23-17-high.pdf

[53] Olugbeji Jemitola, P.: *Conceptual Design and Optimization Methodology for Box Wing Aircraft.* Cranfield, UK : School of Aerospace Engineering, Cranfield University, 2012. – URL https://core.ac.uk/download/pdf/14343135.pdf

Bibliography

[54] PETERSON, S. B. ; APT, J. ; WHITACRE, J. F.: Lithium-Ion Battery Cell Degradation Resulting From Realistic Vehicle and Vehicle-to-Grid Utilization. In: *Journal of Power Sources* 195 (2010), Nr. 8, S. 2385–2392. – ISSN 03787753

[55] PRANDTL, L.: *Induced Drag of Multiplanes: Reproduced for NASA*. NASA Scientific and Technical Information Facility, 1965. – URL https://ntrs.nasa.gov/archive/nasa/casi.ntrs.nasa.gov/19930080964.pdf

[56] RAYMER, Daniel P.: *Aircraft Design: A Conceptual Approach*. 5. Reston, Virginia : American Institute of Aeronautics and Astronautics, Inc, 2012

[57] REDEKER, G. ; WICHMANN, G.: Forward sweep: A favorable concept for a laminar flow wing. In: *Journal of Aircraft* 28 (1991), Nr. 2, S. 97–103. – ISSN 0021-8669

[58] REIST, T. A. ; ZINGG, D. W.: High-Fidelity Aerodynamic Shape Optimization of a Lifting-Fuselage Concept for Regional Aircraft. 54 (2017), Nr. 3, S. 1085–1097. – URL http://oddjob.utias.utoronto.ca/~dwz/Miscellaneous/ReistZinggJofA2016.pdf

[59] RIZZO, E.: *Optimization Methods Applied to the Preliminary Design of Innovative, Non Conventional Aircraft Configurations*. ETS. Pisa, Italien, 2009. – ISBN 978-884672458-8

[60] ROHACS, J. ; ROHACS, D.: *GABRIEL*. 2011. – URL http://www.gabriel-project.eu/

[61] ROSKAM, J.: *Part V: Component weight estimation*. Ottawa, Kansas : Roskam Aviation and Engineering Corporation, 1985

[62] SCHIKTANZ, D.: *Conceptual Design of a Medium Range Box Wing Aircraft*. Hamburg, Deutschland, Department of Automotive and Aeronautical Engineering, Hamburg University of Applied Sciences, Masterarbeit, 2011. – URL http://www.fzt.haw-hamburg.de/pers/Scholz/arbeiten/TextSchiktanzMaster.pdf

[63] SCHIKTANZ, D. ; SCHOLZ, D.: *Box Wing Fundamentals - an Aircraft Design Perspective*. Hamburg, Deutschland : Aero - Aircraft Design and Systems Group, University Of Applied Sciences, 2011. – URL http://www.fzt.haw-hamburg.de/pers/Scholz/Airport2030/Airport2030_PUB_DLRK_11-09-27.pdf

[64] SCHIKTANZ, D. ; SCHOLZ, D.: *The Conflict of Aerodynamic Efficiency and Static Longitudinal Stability of Box Wing Aircraft*. Hamburg, Deutschland : Aero - Aircraft Design and Systems Group, University Of Applied Sciences, 2011. – URL http://www.fzt.haw-hamburg.de/pers/Scholz/Airport2030/Airport2030_PUB_CEAS_11-10-24.pdf

[65] SCHIKTANZ, D. ; SCHOLZ, D.: Das Boxwing-Flugzeug. In: *Ingenieurspiegel* (2012), Nr. 2

[66] SCHÜLTKE, F.: *Übung 01 im Fach Flugzeugbau II: Initial Sizing*. Aachen, Deutschland : Institut für Luft- und Raumfahrtsysteme, RWTH Aachen University, 2017

[67] SCHÜLTKE, F.: *Übung 11 im Fach Flugzeugbau II: Aerodynamik*. Institut für Luft- und Raumfahrtsysteme, RWTH Aachen University, 2017

[68] SCHÜLTKE, F. ; SCHÄFER, K. ; RISSE, K.: *Central Reference Aircraftf data System (CeRAS)*. 2014. – URL http://ceras.ilr.rwth-aachen.de/

[69] SCHÜTT, M. ; HARTMANN, P. ; MOORMANN, D.: *Fullscale Windtunnel Investigation of Actuator Effectiveness during Stationary Flight within the Entire Flight Envelope of a Tiltwing MAV*. Aachen, Deutschland : Institute of Flight System Dynamics, RWTH Aachen University, 2014

Bibliography

[70] STUMPF, E.: *FZB II Übung: Steuerflächen und Hochauftriebshilfen.* Aachen, Deutschland : Institut für Luft- und Raumfahrtsysteme, RWTH Aachen University, 2018

[71] TAAMALLAH, S.: *Optimal Autorotation With Obstacle Avoidance For A Small-Scale Flybarless Helicopter UAV.* Amsterdam, Niederlande : Nationaal Lucht- en Ruimtevaartlaboratorium, National Aerospace Laboratory NLR, 2014

[72] THIELMANN, A. ; NEEF, C. ; HETTESHEIMER, T. ; DÖSCHER, H. ; WIETSCHEL, M. ; TÜBKE, J. ; FRAUNHOFER-INSTITUT FÜR SYSTEM- UND INNOVATIONSFORSCHUNG (Hrsg.): *Energiespeicher-Roadmap (Update 2017): Hochenergie-Batterien 2030+ und Perspektiven zukünftiger Batterietechnologien.* – URL https://www.isi.fraunhofer.de/content/dam/isi/dokumente/cct/lib/Energiespeicher-Roadmap-Dezember-2017.pdf

[73] TORENBEEK, E.: *Synthesis of Subsonic Airplane Design.* Rotterdam : Delft University Press, 1976

[74] URANGA, A. ; DRELA, M. ; GREITZER, E. M. ; HALL, D. K. ; TITCHENER, N. A. ; LIEU, M. K. ; SIU, N. M. ; CASSES, C. ; HUANG, A. C. ; GATLIN, G. M. ; HANNON, J. A.: Boundary Layer Ingestion Benefit of the D8 Transport Aircraft. In: *AIAA Journal* 55 (2017), Nr. 11. – ISSN 0001-1452

[75] VETTERS, D. K. ; KARAM, M. ; FULAYTER, R. D.: *Ultra High Bypass Ratio Turbofan.* Rolls-Royce Corporation and Rolls-Royce North American, 2014

[76] WEINTRAUB, D.: *GasTurb 13.* 2017. – URL http://www.gasturb.de/impressum.html

[77] WELSTEAD, J. R. ; FELDERY, J. L.: *Conceptual Design of a Single-Aisle Turboelectric Commercial Transport with Fuselage Boundary Layer Ingestion.* American Institute of Aeronautics and Astronautics, Inc, 2016. – URL https://ntrs.nasa.gov/archive/nasa/casi.ntrs.nasa.gov/20160007674.pdf

[78] WILFERT, G. ; SIEBER, J. ; ROLT, A. ; BAKER, N. ; TOUYERAS, A. ; COLANTUONI, S.: New Environmental Friendly Aero Engine Core Concepts. (2007). – URL http://citeseerx.ist.psu.edu/viewdoc/download?doi=10.1.1.619.6911&rep=rep1&type=pdf

[79] WOLKOVITCH, J.: The Joined Wing - An Overview. In: *Journal of Aircraft* 23 (1986), Nr. 3. – ISSN 0021-8669

[80] WOROBEL, R. ; MAYO, M. G. ; HAMILTON STANDARD (Hrsg.): *Advanced Genral Aviation Propeller Study.* 1971

[81] YOMCHINDA, T. ; HORN, J. F. ; LANGELAAN, J. W.: *Autonomous Control and Path Planning for Autorotation of Unmanned Helicopters.* Pennsylvania : Department of Aerospace Engineering, The Pennsylvania State University, 2012

[82] ZHAO, X. ; GRÖNSTEDT, T.: *Aero Engine Intercooling Optimization Using a Variable Flow Path.* Göteborg, Sweden : Chalmers University of Technology, 2015. – URL http://publications.lib.chalmers.se/records/fulltext/225382/local_225382.pdf. – ISBN ISABE-2015-20018

[83] ZOHLANDT, C. N.: *Conceptual Design of High Subsonic Prandtl Planes: Analysis and Performance Comparison with Conventional Configurations in the High Subsonic Transport Category.* Delft, Niederlande, Delft University of Technology, Masterarbeit, 2016

A Appendix A

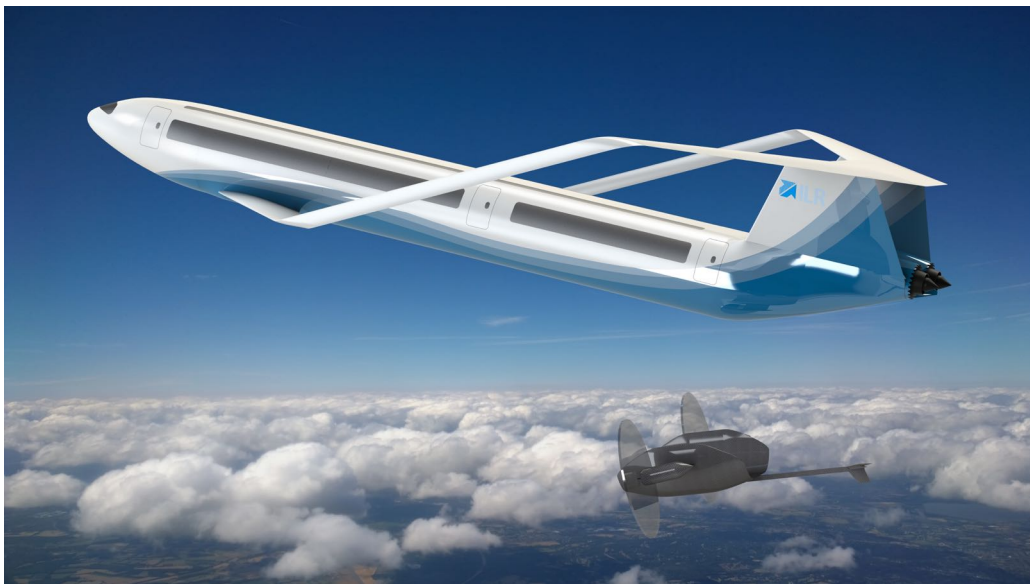

Figure A.1: AixBox Ones flying in formation

Figure A.2: Booster detaching at FL250
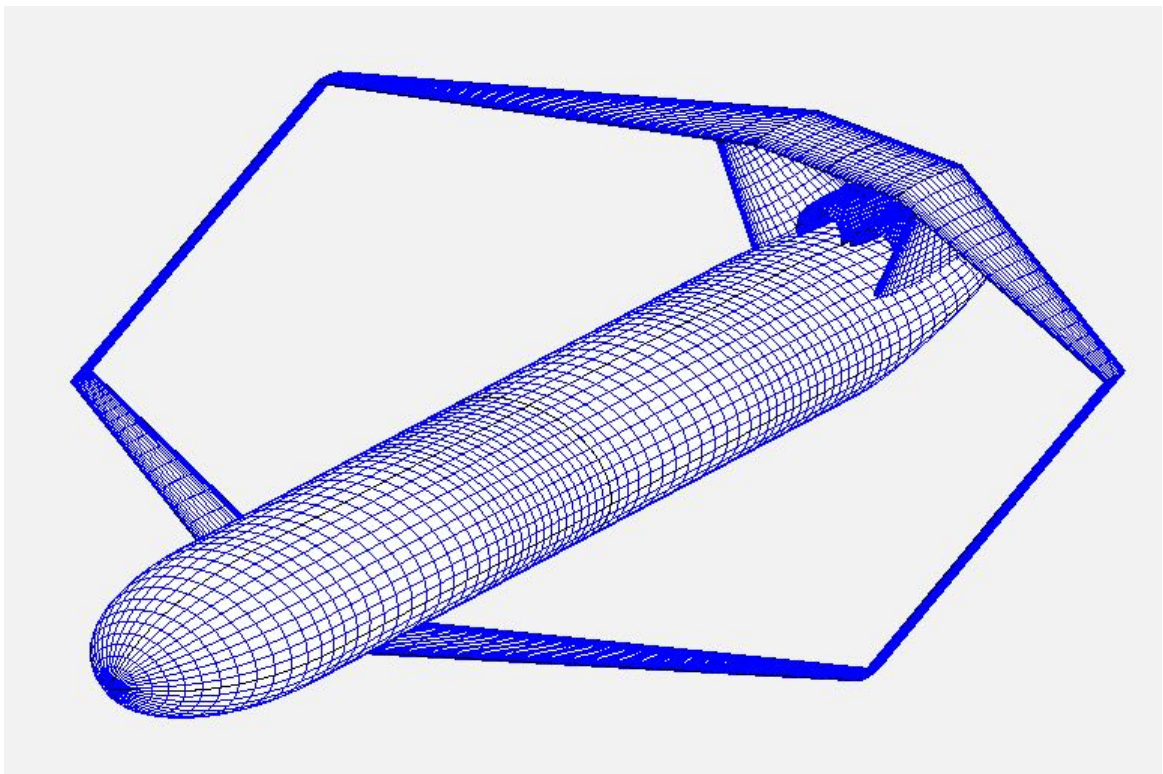
Figure A.3: AixBox One in cruise flight

Figure A.4: OpenVSP mesh of the boxwing

Appendix A. Appendix A

Table A.1: Wing geometric parameters

Parameter		Fore Wing	Aft Wing	Combined	A320
S	m^2	55.90	55.90	111.81	122.4
Λ	-	12.5	12.5	6.25	9.47
b	m	26.43	26.43	-	34.04
λ	-	0.33	0.33	-	0.24
l_{root}	m	3.18	3.18	-	6.05
l_{tip}	m	1.05	1.05	-	1.8
φ	$^\circ$	34	-28	-	25
MAC	m	2.29	2.29	2.29	4.18
x_{LEMAC}	m	11	34.02	-	14.3
ν	$^\circ$	4	0	-	5
h/b	-	-	-	0.25	-
t/c	-	0.1	0.1	0.12	

Table A.2: Wing parameters for stability analysis

Parameter		Fore Wing	Aft Wing
h_0	—	0.25	0.25
s	-	0.5	0.5
$\bar{c}$	m	2.29	2.29
$\bar{c}'$	-	1	1
l'	m	23.02	
$\bar{V}'$	-	5.02	
C_M	-	-0.1	-0.1
$\frac{dC_L}{d\alpha}$	-	5.89	6.14
$\frac{dC_{L2}}{dC_L}$	-	0.97	
$C_{L,cruise}$	-	0.70	0.57
$C_{M,CG}$	-	0.11 > 0	

Table A.3: Empennage geometric parameters

Parameter		AixBox One	A320
b	m	3.89	6.86
Λ	-	0.76	1.67
S_{proj}	m^2	28	28.19
S	m^2	39.6	28.19
λ	-	0.38	0.24
φ	$^\circ$	-33	40.83
l_{root}	m	7.38	7.0
l_{tip}	m	2.8	1.97
MAC	m	5.44	4.58
ν	$^\circ$	45	0

Appendix A. Appendix A

Table A.4: Empennage parameters for stability analysis

Parameter		Design CG	Foremost CG	Rearmost CG
$C_{n\beta}$ fore wing	−	0.0038	0.0038	0.0038
$C_{n\beta}$ aft wing	−	-0.0017	0.0017	0.0017
$C_{n\beta}$ fuselage	−	-0.217	-0.215	-0.231
$C_{Y\beta}$ V-Tail	−	1.119	1.119	1.119
$C_{n\beta}$ CG	−	$0.06 > 0$	$0.07 > 0$	$0.04 > 0$
C_n CG	−	$0.039 > 0$	$0.04 > 0$	$0.036 > 0$

Table A.5: Engine component efficiencies

LPC	IPC	HPC	HPT	IPT	LPT
90 %	93 %	93 %	91 %	92 %	94 %